THE GEOLOGICAL SOCIETY
OF AMERICA®

Vein topology, structures, and distribution during the prograde formation of an Archean gold stockwork

François Turlin[1,†], Stéphane De Souza[1], Michel Jébrak[1], Pierre-Arthur Groulier[1], and Jordi Turcotte[2]
[1]*Université du Québec à Montréal, Département des Sciences de la Terre et de l'Atmosphère, 201, ave. du Président-Kennedy, Montréal, Québec, Canada H2X 3Y7*
[2]*Sirios Resources, Inc., 1000 rue Saint-Antoine Ouest (suite 410), Montréal, Québec, Canada H3C 3R7*

ABSTRACT

The Archean Cheechoo stockwork gold deposit is hosted by a felsic intrusion of tonalitic-granodioritic composition and crosscutting pegmatite dikes in the Eeyou Istchee James Bay area of Quebec, Canada (Archean Superior craton). The evolution of the stockwork is characterized herein using field relationships, vein density, and connectivity measurements on drill core and outcrop zones. The statistical distribution of gold is used to highlight mechanisms of stockwork emplacement and gold mineralization and remobilization.

Two statistical populations of gold concentration are present. Population A is represented by gold grades below 1 g/t with a lognormal cumulative frequency. It is widespread in the hydrothermally altered (albite and quartz) and mineralized facies of the pluton. It is controlled by the development of quartz-feldspar-diopside veins as shown by the similar lognormal distribution of grades and vein density and by the correspondence of grades with network connectivity. Diopside and actinolite porphyroblasts in deformed veins within sodic and calcsilicate alteration zones are evidence for auriferous vein emplacement prior to the amphibolite facies peak of metamorphism.

Population B (>1 g/t) is erratic and exhibits a strong nugget effect. It is present throughout the mineralized portion of the pluton and in pegmatites. This population is interpreted as the result of gold remobilization during prograde metamorphism and pegmatite emplacement following the metamorphic peak. The pegmatites are interpreted to have scavenged gold emplaced prior to peak metamorphism.

These results show the isotropic behavior of the investigated stockwork during regional deformation and its development during the early stages of regional prograde metamorphism.

INTRODUCTION

Fracture and vein network analysis has always been a subject of great interest in geosciences and has applications to petroleum resources, aquifer characterization, and metallogeny (e.g., Narr and Suppe, 1991; Gillespie et al., 1993, 1999; Sanderson et al., 1994, 2008; Roberts et al., 1998, 1999; Monecke et al., 2001; André-Mayer and Sausse, 2007; Hooker et al., 2012, 2013, 2018; Hooker and Katz, 2015; Sanderson and Nixon, 2015; McGinnis et al., 2017; Lavenu and Lamarche, 2018; Watkins et al., 2018). The description of, and interest for, vein and fracture networks has evolved through time with the introduction in the literature of several quantitative parameters for describing and quantifying their distribution. These parameters include vein thickness, length, spacing, and fractal distribution (Narr and Suppe, 1991; Gillespie et al., 1993; McCaffrey and Johnston, 1996; de Joussineau and Aydin, 2007; Laubach et al., 2018; Marrett et al., 2018). They allow the estimations of network density and connectivity in relatively simple systems, i.e., monophased networks that formed in brittle domains and in rocks that underwent low metamorphic grade (e.g., Narr and Suppe, 1991; Gillespie et al., 1993; Hooker et al., 2012, 2013, 2018; Hooker and Katz, 2015; McGinnis et al., 2017; Lavenu and Lamarche, 2018; Roberts et al., 1998, 1999; Sanderson et al., 1994, 2008; Watkins et al., 2018). However, even though a significant proportion of hydrothermal systems are found in crustal segments that undergo ductile-brittle deformation, it is challenging to characterize the vein distribution and connectivity of polyphased vein networks emplaced in high-grade terranes, which underwent subsequent deformation and high-grade metamorphism.

To provide a frame for the investigation of such complex systems, we chose to focus on an Archean stockwork that represents a dense network of well-organized to randomly oriented veins. Stockworks are in some cases polyphased, and they occur in a variety of settings and are a hallmark of numerous metal deposits such as porphyry Cu(-Au) (Ulrich and Heinrich, 2002; Sillitoe, 2010), iron oxide copper gold (IOCG) (Corriveau et al., 2010), and volcanogenic massive sulfide (VMS) deposits (Solomon, 1976; Franklin et al., 1981). They are usually formed during the progressive cooling of the magmatic-hydrothermal components. In Archean greenstone belts of the Superior craton, numerous stockworks have been described, such as those of the Don Rouyn, Coté Gold, and Troilus gold deposits (Jébrak, 1992; Fraser, 1993; Goodman et al., 2005; Katz et al., 2017). In the case of these magmatic-hydrothermal systems, there is commonly a significant hiatus between the emplacement of the gold-rich stockwork associated with the cooling of the pluton and later superimposed deformation and metamorphism that affect the host rocks. However, in the James Bay area, the Cheechoo gold deposit displays an exceptional setting where the stockwork formation appears to be closely associated with prograde metamorphism, but emplacement mechanisms remain poorly constrained (Fontaine et al., 2018; Turlin et al., 2019b).

The Cheechoo gold deposit (93 Mt of ore grading at 0.65 g/t Au for a total of 1.95 million ounces (Moz) of gold resources; data from Sirios Resources, Inc., November 2020) is located in the Eeyou Istchee James Bay area of Quebec, Canada, which is part of the Archean Superior craton. It is characterized by a stockwork hosted within a pluton of tonalitic to granodioritic composition emplaced within metasedimentary rocks. At Cheechoo, the veins that host the mineralization were affected by polyphase

François Turlin https://orcid.org/0000-0002-0378-6972

[†]Present address: Department of Earth Sciences, University of Geneva, Rue des Maraîchers 13, 1205 Geneva, Switzerland; francois.turlin@unige.ch.

GSA Bulletin; https://doi.org/10.1130/B36057.1; 10 figures; 2 tables; 1 supplemental file.

deformation during compressional and late-tectonic events (D_2 and D_3), metamorphosed up to upper amphibolite facies conditions, and cut by syn- to late-kinematic granitic pegmatites (Fontaine et al., 2018; Fontaine, 2019; Turlin et al., 2019b).

Turlin et al. (2019b) explored the vertical variations of the network distribution and topology of the various hydrothermal and pegmatitic vein networks that form the deposit and addressed the reliability of these approaches for characterizing vein networks that underwent subsequent high-grade metamorphism. The gold mineralization appears to be mainly controlled by (1) the density of quartz-feldspar-diopside (Qtz-Fsp-Di) and quartz (Qtz) veins and by (2) the connectivity of these networks as shown by the increase of both parameters with increasing gold grade. The topologic approach allows a direct estimation of the vein network connectivity at the time of vein formation (Sanderson and Nixon, 2015, 2018), can characterize vein networks in hydrothermal systems (Turlin et al., 2019b; Blenkinsop et al., 2020), and can be used as a proxy for the prediction of metal grade when applied to metal deposits (Turlin et al., 2019b).

In this study, we explore evolution of the Cheechoo stockwork over space and time and whether vein connectivity, density, and topology are consistent in three dimensions. We also investigate how the geometry and topology of the Cheechoo stockwork changed during its evolution in a prograde metamorphic environment. This work allows us to (1) define the methodologies to be used for the description, characterization, and interpretation of vein networks affected by high-grade metamorphism and to (2) understand the evolution of vein connectivity in a prograde stockwork and its relation to metamorphism.

We used detailed mapping and structural analysis of a large, stripped outcrop and quantified vein density, topology, connectivity, and gold grade distribution to identify mechanisms of vein emplacement. This study provides new tools for the characterization of vein networks, especially in metal deposits, and allows for a better understanding of stockwork formation and evolution during prograde metamorphism at amphibolite facies conditions.

GEOLOGICAL FRAMEWORK

Regional Setting

The Cheechoo intrusion is located in the La Grande subprovince close to the contact with the Opinaca subprovince (Fig. 1B). The Opinaca subprovince consists of Neoarchean migmatitic paragneiss, diatexite, and amphibolite (Simard and Gosselin, 1999; Bandyayera and Fliszár, 2007; Bandyayera and Lacoste, 2009; Bandyayera et al., 2010; Cleven et al., 2020) intruded by granodiorite, granite, and pegmatite plutons and dikes (Bandyayera and Fliszár, 2007; Bandyayera and Lacoste, 2009). In the study area, the La Grande subprovince consists of polyphased diorite, tonalite, granodiorite, and granite intrusions emplaced into Neoarchean volcanic and sedimentary rocks of the Eastmain Group (ca. 2734–2686 Ma; Moukhsil, 2000; Moukhsil et al., 2003; Bandyayera and Fliszár, 2007; Bandyayera and Lacoste, 2009; Bandyayera et al., 2010; David et al., 2010; Ravenelle et al., 2010; Fontaine, 2019). The Eastmain Group consists of the Bernou and Kasak formations, which are composed of basalt and andesite with a tholeiitic to calc-alkalic affinity (Moukhsil, 2000; Moukhsil et al., 2003; Bandyayera and Fliszár, 2007; Bandyayera and Lacoste, 2009; Bandyayera et al., 2010) and of wacke and polymictic conglomerate belonging to the Pilipas and Low formations (Bandyayera and Fliszár, 2007; Bandyayera and Lacoste, 2009; Bandyayera et al., 2010; David et al., 2010; Ravenelle et al., 2010). The Low Formation is the main host of the Cheechoo intrusion, and it is mainly represented by turbiditic wacke locally grading into pelitic sillimanite-bearing paragneiss. The wacke also contains metamorphosed volcaniclastic rock horizons, iron formations, and skarn-like metamorphic and/or hydrothermal assemblages, where garnet-biotite-amphibole-epidote bands locally define the metamorphic layering (Fontaine et al., 2018). Syn- to late-tectonic Neoarchean intrusions, such as the Cheechoo intrusion, were emplaced into these supracrustal sequences (Ravenelle et al., 2010; Dubé et al., 2011; Fontaine et al., 2015). All of these Archean units from the La Grande and Opinaca subprovinces were subsequently crosscut by Paleoproterozoic diabase dikes (between ca. 2491 Ma and 2208 Ma; Fahrig et al., 1986; Buchan et al., 1993; Heaman, 1997).

Structures and Metamorphism

Four main phases of deformation were recognized in the La Grande subprovince in the area covering the Cheechoo deposit (Ravenelle, 2013; Morfin et al., 2013; Fontaine et al., 2018). D_1 is bracketed between 2710 Ma and 2697 Ma based on U-Pb zircon dating of syn-tectonic plutons (Moukhsil, 2000; Moukhsil et al., 2003; Bandyayera et al., 2010). D_1 is cryptic and associated with F_1 folds that are overprinted by F_2 folds (Bandyayera et al., 2010; Ravenelle et al., 2010). D_2 is the main phase of deformation and can be bracketed between 2675 Ma and ca. 2605 Ma (Moukhsil et al., 2003; Bandyayera and Fliszár, 2007; Bandyayera et al., 2010; Ravenelle, 2013; Fontaine et al., 2015; Fontaine, 2019). It is characterized by a N-S compressional event and by the transposition of bedding and of the S_1 into the S_2 foliation, which is axial-planar to F_2 folds (Fig. 1; Bandyayera et al., 2010). D_3 is characterized by SW-NE–trending F_3 folds and associated with the formation of a dome-and-basin interference pattern (Fig. 1B; Remick, 1977; Ravenelle et al., 2010) that is attributed to a late tectonic episode of intrusion emplacement (Ravenelle et al., 2010) that also affected the orientation of the S_2 foliation (Bandyayera et Fliszár, 2007; Ravenelle et al., 2010; Fontaine et al., 2017). The S_3 foliation is marked by the reorientation of aluminosilicate porphyroblasts in the metasedimentary rocks, by the development of a crenulation cleavage associated with F_3 folds, and by the local reorientation of F_2 folds concentrically around late tectonic intrusive domes (Bandyayera et al., 2010). D_4 is marked by E-W– to NW-SE–trending subvertical faults and high strain zones (Fig. 1B; Morfin et al., 2013; Fontaine et al., 2018).

In the La Grande subprovince, metamorphic grade increases toward the east and from south to north in the area surrounding the Cheechoo intrusion. Metamorphism ranges from greenschist to upper amphibolite facies conditions and reaches upper amphibolite facies along the contact with the Opinaca subprovince ($\sim$650 °C, $\sim$5–6 kbar) (Bandyayera et al., 2010; Ravenelle et al., 2010; Fontaine, 2019). In the Opinaca subprovince, metamorphic conditions increase toward the south and reach granulite facies close to its southern margin (Simard and Gosselin, 1999; Bandyayera et al., 2010; Côté-Roberge, 2018). Partial melting in the Opinaca subprovince occurred between ca. 2666 Ma and 2636 Ma based on U-Pb dating of zircon from migmatites and leucogranite dikes (Morfin et al., 2013). This episode of migmatization is interpreted as syn-D_2 based on the presence of syn-kinematic dikes. The migmatite displays asymmetric folds (Morfin et al., 2013, 2014) and mutual crosscutting relationships with the S_2 fabric (Ravenelle et al., 2010). Recent studies have shown that the Opinaca subprovince experienced an earlier high-temperature and low-pressure metamorphic event around 2670–2660 Ma that was followed by a high-temperature and medium-pressure metamorphic event at ca. 2645 Ma (Cadéron, 2003; Morfin et al., 2013, 2014; Côté-Roberge, 2018).

The Cheechoo Intrusion

The Cheechoo intrusion is composed of metaluminous granodiorite and tonalite, which composition indicates reduced conditions (Fontaine et al., 2018). A sample collected on the main stripped outcrop yielded an age of ca.

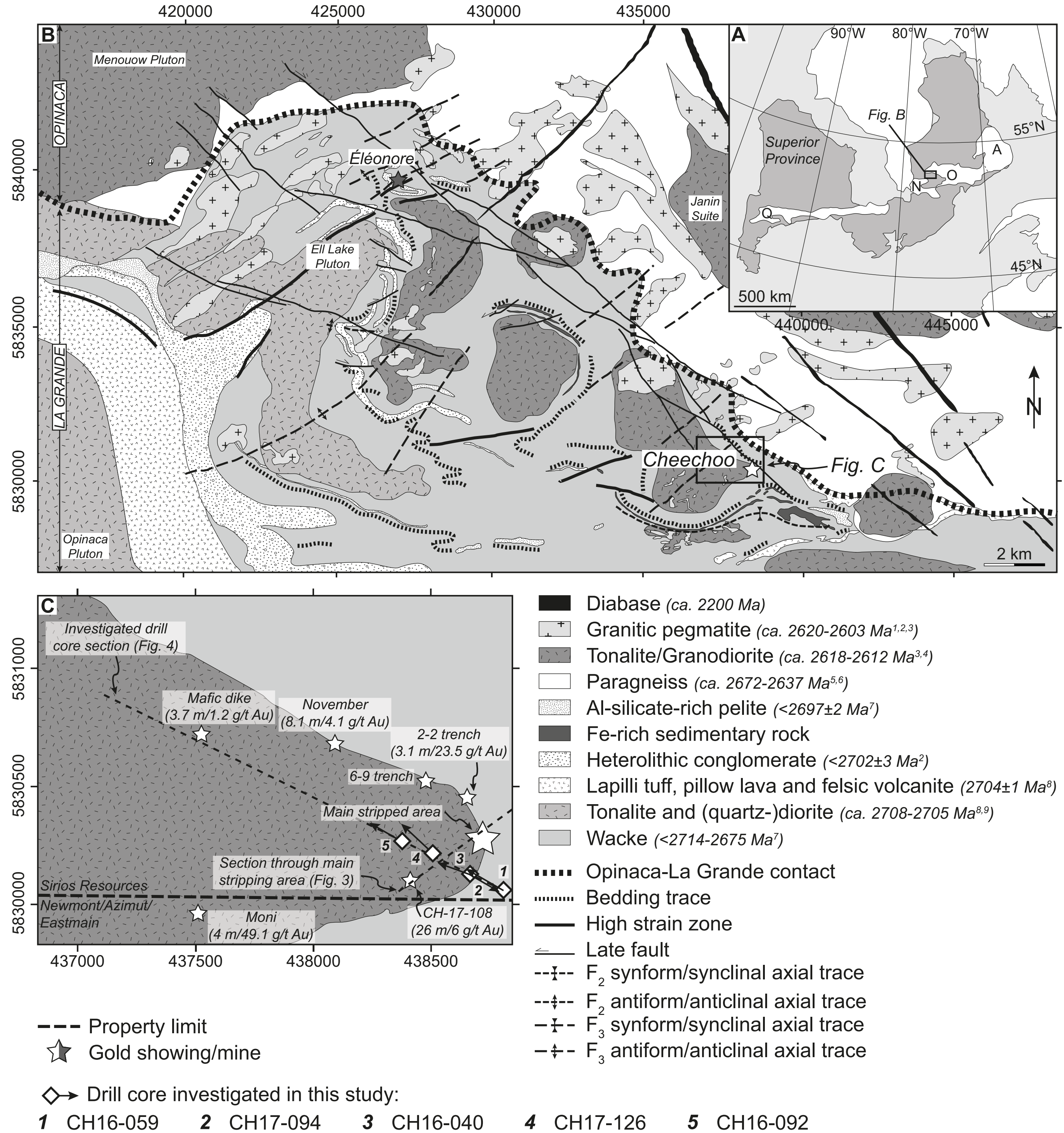

Figure 1. (A) Positions of the Superior Province and the Quetico, Nemiscau, Opinaca, and Ashuanipi subprovinces in North America are shown (after Fontaine et al., 2017, 2018). (B) Geological map of the Cheechoo intrusion area (Eeyou Istchee James Bay, Québec) and position of the Cheechoo gold showing that was investigated in this study in the frame of the La Grande and Opinaca subprovinces (after Fontaine et al., 2017, 2018). (C) Simplified location map showing the main gold occurrences belonging to the Cheechoo gold deposit and the trace of the drill cores investigated in this study (after Fontaine et al., 2018). Abbreviations: 1—Dubé et al. (2011); 2—Ravenelle et al. (2010); 3—Fontaine et al. (2015); 4—Goutier et al. (2000); 5—David et al. (2010); 6—Morfin et al. (2013); 7—McNicoll (unpublished data reported in Fontaine et al., 2017, 2018); 8—Bandyayera and Fliszár (2007); 9—David (unpublished data reported in Fontaine et al., 2017, 2018); A—Ashuanipi; N—Nemiscau; O—Opinaca; Q—Quetico. Coordinates: NAD83, UTM 18N zone.

2612 Ma that is interpreted as the crystallization age (U-Pb thermal ionization mass spectrometry (TIMS) on zircon; Fontaine et al., 2015). The intrusion has undergone high-grade metamorphism and intense hydrothermal alteration mainly albitization. It is mainly composed of quartz-feldspar-biotite ± diopside ± actinolite with feldspar phenocrysts and biotite porphyroblasts (Fontaine et al., 2018). Textures range from massive and saccharoidal to strongly foliated. The surrounding wacke is intruded by apophyses of the Cheechoo intrusion, and both the wacke and the intrusion are crosscut by numerous granitic pegmatite dikes (Fontaine et al., 2018). The contact between the intrusion and the wacke is often marked by E-trending isoclinal F_3 folds and numerous pegmatite dikes and veins as described in the 6–9 trench (Fig. 1C) by Fontaine et al. (2018). On the main stripped area, the contact is either sharp, obscured by the emplacement of a mafic dike and pegmatites, or overprinted by a syn-D_3 shear zone and a late subvertical fault (Fig. 2A).

Several vein types have been reported (Fontaine et al., 2018; Turlin et al., 2019b) from drill core investigations (Table 1). A dominant type is represented by quartz-feldspar-diopside (Qtz-Fsp-Di) veins that, along with a less dominant quartz (Qtz) vein population, have been shown to exert strong control on gold mineralization (Turlin et al., 2019b). The intrusion, S_2 foliation, and gold-related veins are crosscut by pegmatitic dikes, extensional Qtz veins, and chlorite (Chl)-coated fractures (Fontaine et al., 2018; Turlin et al., 2019b).

METHODOLOGY

Structural Analysis

In this study, structural analysis was carried out on both the main stripped area that has been mapped in detail by Sirios Resources, Inc., and by Fontaine et al. (2018) and on drill core sections modeled by Sirios Resources, Inc. The main stripped area is a shallowly inclined surface where large flat zones locally prevent reliable structural measurements. Where possible, the strike and dip of structures and veins (following the right-hand rule) were reported from the main stripped area (Tables S1 and S2[1]) and were used to reconstruct the structural evolution of this area. The outcrop was divided into structural domains, which were based on changing lithologies, facies, or structural pattern (Fig. 2A).

Selected Vein Populations and Drill Cores

A comparison between gold grade values and vein network parameters such as vein density and connectivity allows for a better understanding of these parameters and their influence on fluid circulation and metal concentration. Accordingly, we focused our study on veins that control the gold mineralization, namely, the Qtz-Fsp-Di veins and the Qtz veins (Turlin et al., 2019b). Network parameter measurements and gold grade distribution were investigated on the NW-SE–trending drill core section that is close to the main stripped area (Fig. 1C). This methodology allows for reliable comparisons between the observations carried out on the outcrop and on drill cores, on which the topological characterization of vein networks has already been tested (Turlin et al., 2019b). Along this section, five drill cores (NQ is ~4.7 cm in diameter) with high recovery rates (>99%) were investigated for the quantification of vein density and topology and the distribution of gold grade. Lengths of drill core halves ranging from 0.1 m to 2.0 m were systematically sampled by Sirios Resources, Inc., and analyzed by fire assay at Actlabs and ALS laboratories. The drill cores from NW to SE are: CH16-092, CH17-126, CH16-040, CH17-094, and CH16-059 (Figs. 1C and 3). Their azimuths, dips, and lengths are reported in Table 2.

The gold grades were used to interpolate gold grade envelopes on drill core sections. The interpolation was carried out by Sirios Resources, Inc., using the Leapfrog radial basis function (RBF) tool and by including the orientation of the S_2 foliation for better determination of envelop geometry. The samples are composited at lengths of 3 m, and the interpolation method uses a half spheroidal variogram. The parameters were set to sill = 25, range = 100, nugget = 3.

Systematic measurements of vein parameters (number and topology) were carried out on the whole length of the intrusion intercepted by the drill cores, and the latter were investigated as 1-D scanlines. These systematic measurements allow comparison of every facies of the pluton including barren and mineralized zones. The intervals considered correspond to those in which gold grade has been analyzed and range in length from 0.1 m to 2.0 m. The results are reported in Table S3 (see footnote 1). Unfortunately, the drill cores investigated were not oriented and did not allow the measurement of the true vein orientations.

Vein Density Measurement

The systematic measurement of density (number of veins per meter) was carried out on selected sections of drill cores. The length of the intervals was corrected by subtracting the thickness of late pegmatites, which are younger than the vein populations investigated. Accordingly, the number of veins obtained on these corrected intervals represents the best estimation of vein density.

The vein populations considered in this study are not subparallel to one another (Turlin et al., 2019b). Therefore, the Terzaghi correction was not applied. This correction aims to yield the most accurate number of veins in the area or volume investigated so the most representative vein density can be calculated. It must only be applied in the case of subparallel veins that would be intersected at low angle with the scanline (Terzaghi, 1965). On the contrary, in the case of vein surveys carried out in areas where a great variety of orientations is available for examination, the variability of orientation likely represents a fair sample of the veins present in the zone investigated (Terzaghi, 1965). Accordingly, the wide spread of θ angles (angle between a vein and the drill core) allows a reliable estimation of their density (Turlin et al., 2019b). The results are reported according to the measured intervals as the number of veins per meter in Table S3 along with the associated gold grade.

Topological Measurements

The topological characterization of veins was carried out following the method of Sanderson and Nixon (2015, 2018), which was demonstrated to be reliable when applied to stockworks that underwent high-grade metamorphism by Turlin et al. (2019b). It involves the counting of node types for each vein from a given population (Manzocchi, 2002; Mäkel, 2007; Sanderson and Nixon, 2015). Three types of nodes can be represented, either isolated tips (I), crossing veins (X), or abutments and splays (Y) (Manzocchi, 2002). The difference in network topologies is a function of the relative node proportion (Sanderson and Nixon, 2015, 2018). The average number of connections per branch (C_B) varies between 0 and 2 and is a direct quantification of the connectivity of the networks (Sanderson and Nixon, 2015, 2018). Its calculation is summarized in Appendix A. We measured the number of each node type for both Qtz-Fsp-Di and Qtz veins on every drill core interval investigated. The points where veins extend across the core were not counted as I nodes but were treated as edge nodes and thus were not included in the calculations. The

[1]Supplemental Material. Structural features investigated on the Cheechoo tonalite/granodiorite including the topological measures carried out on the outcrop and on drill cores, along with the gold grades and facies variability, and the structural measures of foliation and veins from the main stripped area. Please visit https://doi.org/10.1130/GSAB.S.14717937 to access the supplemental material, and contact editing@geosociety.org with any questions.

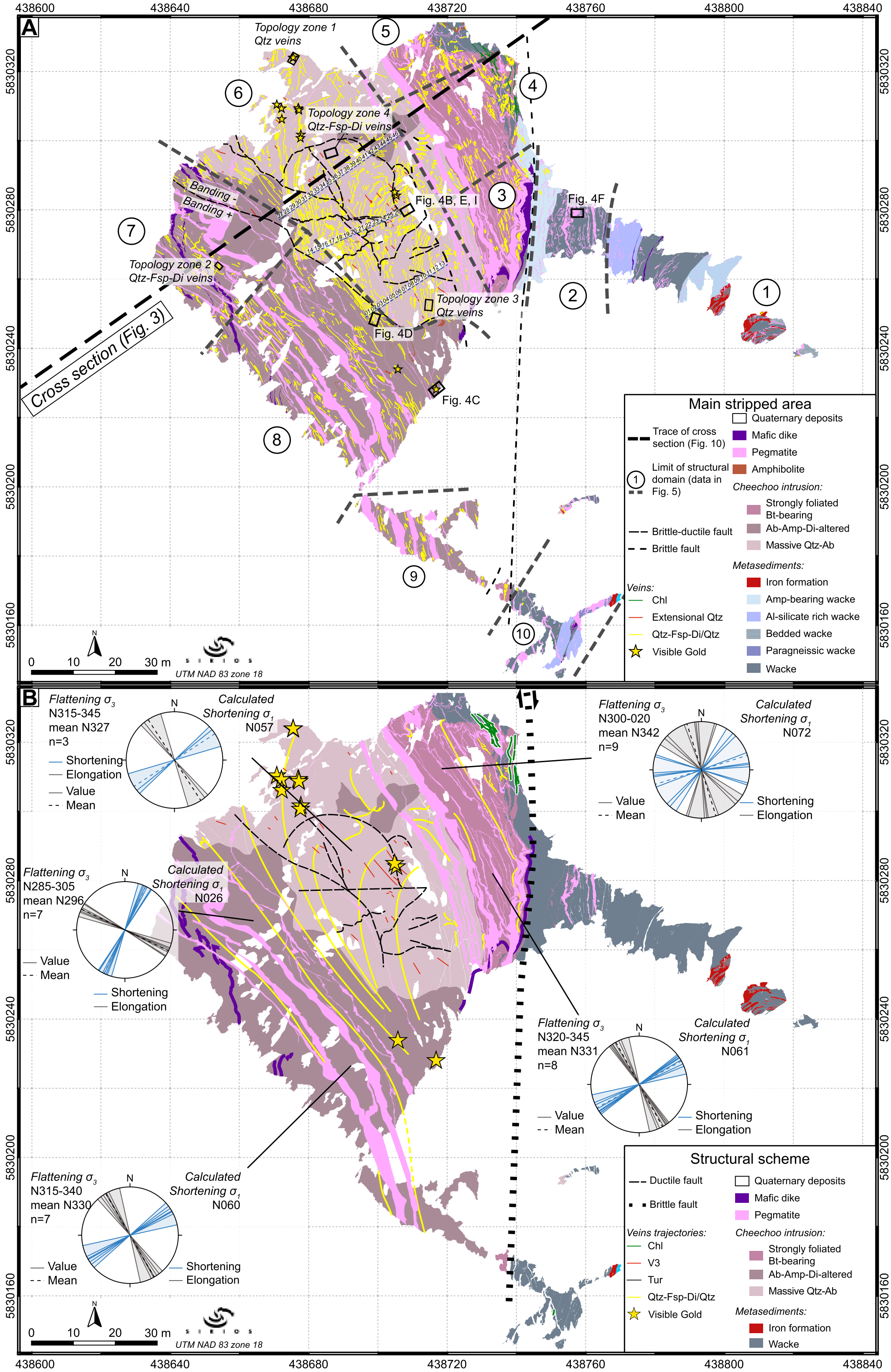

Figure 2. (A) Detailed map shows the main stripped area of the Cheechoo pluton. The trace of the cross section presented in Figure 3, the limits and numbers of structural zones used in Figure 6, the positions of the structural transects presented in Figure S4 (see footnote 1) and of the zones of topological measures presented in Figure 8 that were carried out on the main stripped area are reported. (B) Structural scheme of the main stripped area of the Cheechoo pluton. Abbreviations: Amp—amphibole; Chl—chlorite; Di—diopside; Fsp—feldspar; Qtz—quartz.

results obtained on drill cores include vein topology and connectivity and are reported according to their measured intervals in Table S3 along with the associated gold grade and vein density. Similarly, 2-D zones of several square meters of the central and western parts of the main stripped area were chosen to investigate the topology of Qtz-Fsp-Di and Qtz veins. Veins that extend across the area were treated

TABLE 1. SUMMARY OF THE CHARACTERISTICS OF THE VEIN TYPES OBSERVED IN THE CHEECHOO PLUTON

Vein type	Mineralogy	Width	Relationships with previous veins/structures	Structure/texture	Facies
Qtz-Fsp-Di veins	Qtz-Fsp-Di ± Act ± Scl complemented with Py-Po-Apy ± visible gold Di-Act-Ab centimeter halo	millimeter to centimeter		Systematic alteration halo (1:1 to 1:3 vein over halo ratio) Generally transposed into the S_2 foliation, some are folded and/or dismembered Variable orientations on the main stripped area	Ubiquitous in the intrusion More abundant in most altered facies
Qtz veins	Qtz ± sulfides (Py, Apy, Po)	millimeter to <1 mm	Crosscut Qtz-Fsp-Di veins	Locally present a whitish alteration halo (1:1 vein over halo ratio) Transposed in the S_2 foliation, ptygmatic folded or crosscutting the foliation Generally clustered	Ubiquitous in the intrusion More abundant in most altered facies
Tur veins	Fsp-Tur ± Ttn ± Scl	centimeter	Unobserved	Form ductile breccias	Observed in the Qtz-Ab facies of the main stripped area No link with the Au mineralization
Pegmatitic veins and pegmatites	Qtz-Fsp (pegmatitic veins) ± Bt ± Tur ± Ap ± sulfides (mainly Py ± Cp in pegmatites) Locally present Act-Fsp selvages	centimeter to decimeter (veins) decimeter to decameter (dikes)	Crosscut Qtz-Fsp-Di and Qtz veins	Textural continuity between pegmatitic veins and pegmatite forms a sheeted vein array subparallel or at low angle with the intrusion margins High angle or sub-parallel to S_2 Syn-kinematically folded by F_3 in some places	No links with facies More abundant at the contacts between the intrusion and the wacke
Extensional Qtz veins	Qtz	centimeter to decimeter (veins)	Crosscut Qtz-Fsp-Di and Qtz veins	Extensional veins N- to N-NW–striking perpendicular or sub-parallel to the intrusion margins High to low angle to S2 Perpendicular to high angle to F3 axial planes	Observed in the (sub-) fresh facies of the main stripped area
Chl veins	Chl ± Qtz ± Ep minor Py ± visible gold (rare) (commonly barren)	<1 mm to a few mm	Crosscut every vein type and structures	Straight, unfolded and long (up to decimeter) veins	Ubiquitous in the intrusion May be found in the wacke

Notes: Modified after Fontaine et al., 2018; Turlin et al., 2019b. Abbreviations: Ab—albite; Act—actinolite; Ap—apatite; Apy—arsenopyrite; Bt—biotite; Chl—chlorite; Cp—chalcopyrite; Di—diopside; Ep—epidote; Fsp—feldspar; Po—pyrrhotite; Py—pyrite; Qtz—quartz; Scl—scheelite; Ttn—titanite; Tur—tourmaline.

as edge nodes. The results are reported in Table S4 (see footnote 1).

LITHOLOGIES, FACIES, AND VEIN TYPES

The Cheechoo tonalite to granodiorite intrusion (further designated as granodiorite for the purpose of this article) shows several facies that range from massive quartz-albite-dominated (Fig. S2D; see footnote 1) to several types of more or less penetrative hydrothermal alteration (Fontaine et al., 2018; Turlin et al., 2019b) that range from an albite-amphibole-diopside-altered (Ab-Amp-Di) facies to a biotite-bearing (Bt) facies. The intrusion is also crosscut by several mafic dykes of various orientations. All of these facies and lithologies were affected by the regional metamorphic D_2 compressional event as shown by the development of a penetrative S_2 schistosity. A thorough description of the lithologies and facies that compose the Cheechoo deposit is given in the supplemental file.

Quartz-Feldspar-Diopside Veins

Quartz-feldspar-diopside (Qtz-Fsp-Di) veins are thin (millimeter to centimeter thick). They also contain amphibole, biotite, pyrite, arsenopyrite, pyrrhotite, locally scheelite, and rare visible gold (Figs. 2A and 4A–4C). They are associated with a halo of albite (1:1–1:3 vein over halo ratio). Their orientation is variable on the main stripped area (Fontaine et al., 2018). The veins were transposed into the S_2 foliation (Fig. 4B) and folded during D_2, which locally formed ptygmatic folds (Fig. 4A; Fontaine et al., 2018; Turlin et al., 2019b). Accordingly, we interpret these veins as early- to syn-D_2 (Turlin et al., 2019b).

Quartz Veins

Quartz (Qtz) veins are thin (millimeter to centimeter thick) quartz ± pyrite-arsenopyrite-pyrrhotite ± visible gold veins (Figs. 4D–4E). A halo of albite is locally associated with these veins (1:1–1:2 vein over halo ratio), which have a variable orientation on the main stripped area (Fig. 2A; Fontaine et al., 2018). They are locally found crosscutting the Qtz-Fsp-Di veins, transposed into parallelism with the S_2 foliation, crosscutting the S_2 foliation, or folded. When folded, the Qtz veins locally form ptygmatic folds with a centimeter wavelength (Turlin et al., 2019b). We also interpret these veins as early- to syn-D_2 (Turlin et al., 2019b).

Pegmatites

Pegmatites include centimeter- to meter-wide dikes (Figs 4F, 4G, and 5). They are composed of quartz, plagioclase, and microcline and are therefore of granitic composition (Figs. 4F, 4G, and 4J). They also contain biotite ± tourmaline ± muscovite ± apatite ± pyrrhotite ± pyrite ± chalcopyrite ± rare visible gold and locally garnet where they are intruded into metasedimentary rocks. They are not associated with any sign of contact metamorphism. The pegmatites vary from coarse grained and equigranular to pegmatitic with local graphic textures. In some cases, they have a peculiar texture that is composed of rounded subhedral centimetric quartz phenocrysts and interstitial plagioclase and microcline. This texture, introduced by Turlin et al. (2019b), is referred to as a "giraffe" facies (Fig. 4H). This specific facies is systematically gold-bearing, whereas more typical pegmatite has erratic and random gold values (Turlin et al., 2019b). Relics of altered and randomly foliated host rock with diffuse boundaries are locally found in pegmatites, which suggests that these are partially digested xenoliths (Turlin et al., 2019b).

Pegmatites can be found at high angle or sub-parallel to S_2 (Figs. 2A and 6). They show boudinage, layer-parallel stretching, Z-folding, and local dismembering along fold limbs Moreover, no apparent intracrystalline or solid-state planar fabric indicative of an intense metamorphic recrystallization during deformation can be recognized (Turlin et al., 2019b). This suggests that pegmatite emplacement postdates the syn-D_2 metamorphic fabric, although the

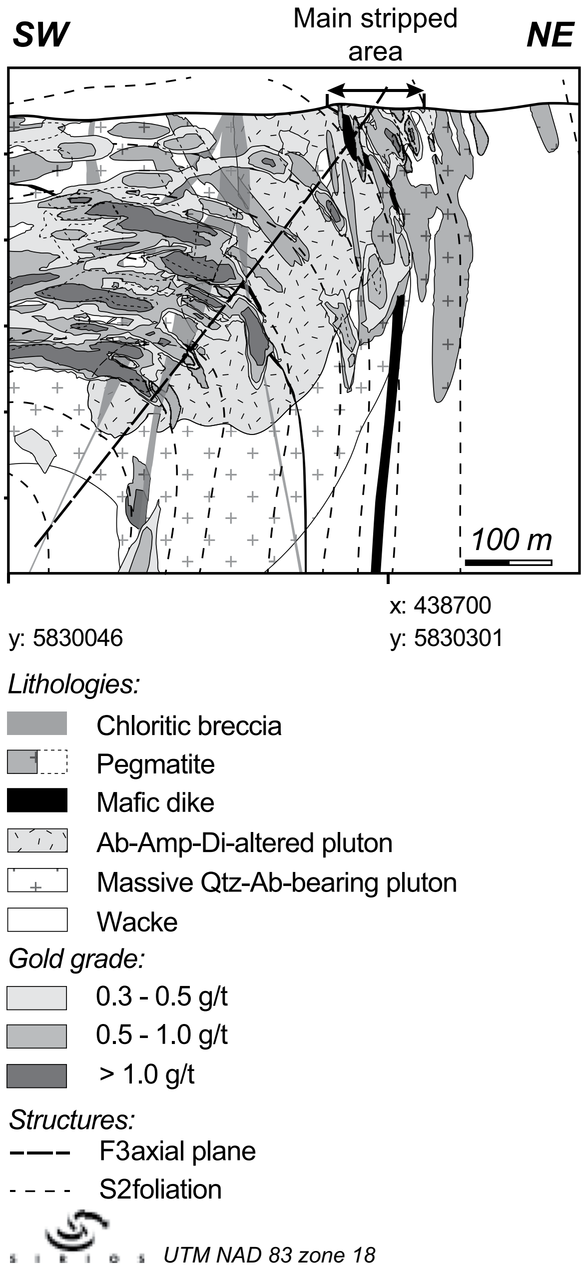

Figure 3. SW-NE cross section across the Cheechoo pluton passes through the main stripped area (modeled from drill core data by Sirios Resources, Inc.). The trace of the cross section is represented in Figure 1C. Note the decrease of gold grade background values in the albite-amphibole-diopside altered pluton and the strike of pegmatites that steepens from SW to NE.

TABLE 2. COORDINATES, STRIKE, DIP, AND LENGTH OF THE DRILL CORES FROM THE CHEECHOO PLUTON INVESTIGATED IN THIS STUDY

Drill core number	Easting*	Northing*	Strike (°)	Dip (°)	Length (m)
CH16-040	438666	5831047	295	–55.00	355.4
CH16-059	438815	5830061	300	–53.00	450.0
CH16-092	438372	5830320	300	–50.00	225.0
CH17-094	438666	5830148	120	–80.00	505.2
CH17-126	438507	5830217	313	–55.00	454.0

Notes: Their respective locations are reported on Figure 1C and the cross section modeled using these drill cores by Sirios Resources, Inc., is represented in Figures 5 and S3 (see footnote 1).
*Coordinates are reported as Universal Transverse Mercator (UTM), in UTM zone 18, projected in the NAD83 system.

pegmatitic veins are affected by ptygmatic F_2 folds (Figs. 4F–4G). Altogether, these features indicate that pegmatites represent syn-kinematic injections that can be bracketed to be late D_2 to early D_3.

Extensional Quartz Veins

A second type of quartz vein consists of extensional lenticular quartz veins up to a few centimeters wide (Fig. 4I). These veins are commonly barren and are either perpendicular (e.g., 6–9 trench) or subparallel to the intrusion margins (main stripped area) (Fontaine et al., 2018). They are essentially exposed in the central part of the main stripped outcrop where they are NW-SE–trending and have a steep dip (80–85°) (Figs. 2 and S4; see footnote 1). They are perpendicular or at high angle to the axial plane of F_3 folds (Fig. 2A).

Chlorite Veins

Chlorite (Chl) veins are straight unfolded and essentially barren chlorite-coated fractures no larger than a few millimeters (Fig. 4J; Fontaine et al., 2018; Turlin et al., 2019b). Even though they are essentially composed of chlorite with local sulfides and rare visible gold particles (Fontaine et al., 2018), Turlin et al. (2019b) demonstrated that they do not exert any control on the gold mineralization. These fractures crosscut the intrusion following a general N-S direction. They crosscut all ductile structural fabrics and the Qtz-Fsp-Di and Qtz veins and pegmatites (Fig. 4J; Fontaine et al., 2018; Turlin et al., 2019b). These features and their mineralogy demonstrate their late emplacement under brittle conditions.

STRUCTURES

Foliations, Folds, Dikes and Faults

The main stripped area consists of an outcrop where the Cheechoo intrusion and the host metasedimentary rocks are both exposed (Fig. 2A). The contact between both units is sharp and locally masked by mafic dikes or pegmatites. The metasedimentary rocks consist of massive to bedded wacke, sillimanite-rich metapelite, and silicate facies iron formation (garnet-amphibole) (Fig. 2A). Large rafts of amphibole-bearing wacke are also present within the intrusion.

Sedimentary bedding (S_0) is NW-striking and steeply dipping toward the NE or SW (structural domain 1; Figs. 2A and 6). Graded bedding is locally preserved and indicates an eastward-younging sedimentary sequence (structural

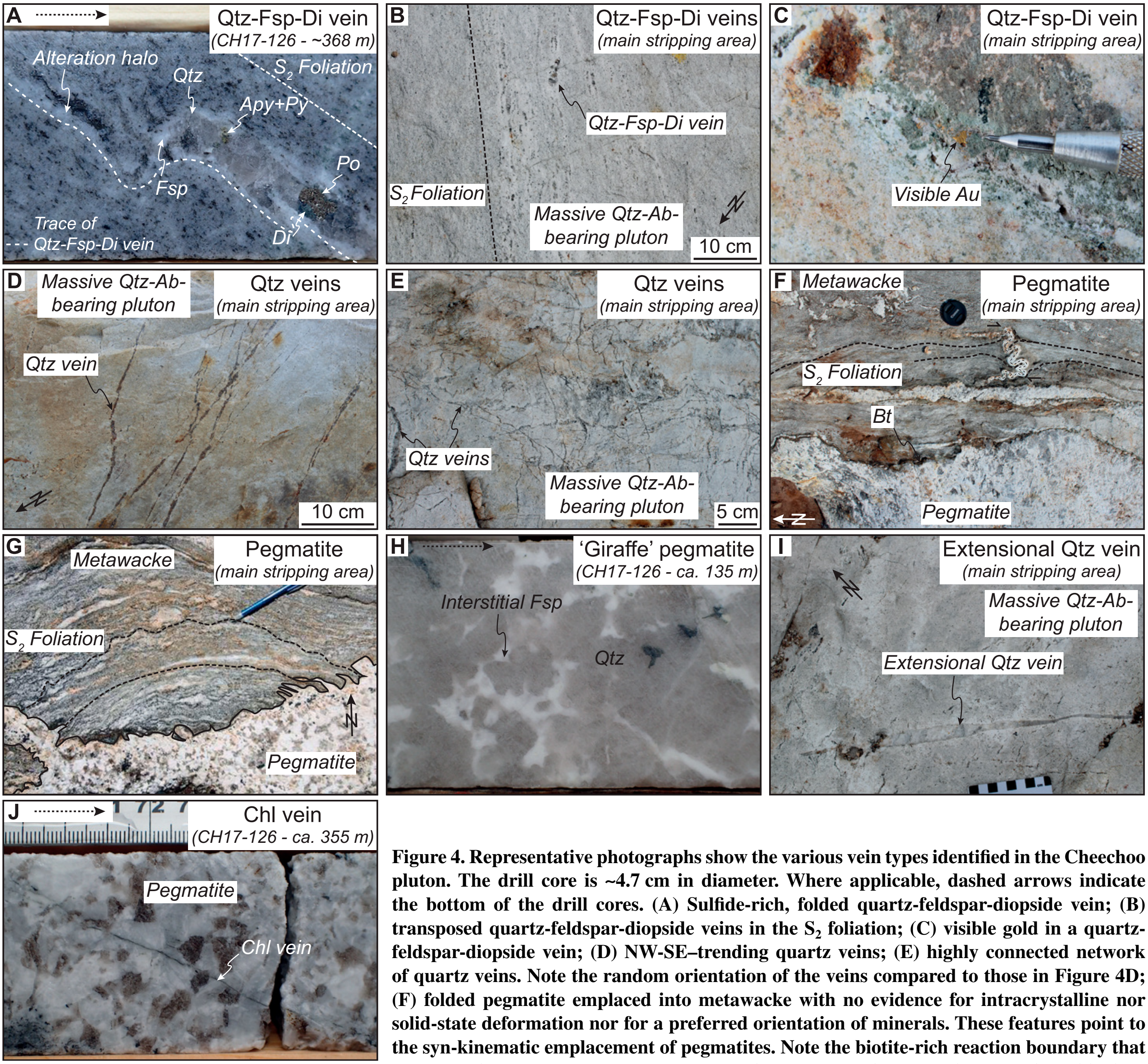

Figure 4. Representative photographs show the various vein types identified in the Cheechoo pluton. The drill core is ~4.7 cm in diameter. Where applicable, dashed arrows indicate the bottom of the drill cores. (A) Sulfide-rich, folded quartz-feldspar-diopside vein; (B) transposed quartz-feldspar-diopside veins in the S_2 foliation; (C) visible gold in a quartz-feldspar-diopside vein; (D) NW-SE–trending quartz veins; (E) highly connected network of quartz veins. Note the random orientation of the veins compared to those in Figure 4D; (F) folded pegmatite emplaced into metawacke with no evidence for intracrystalline nor solid-state deformation nor for a preferred orientation of minerals. These features point to the syn-kinematic emplacement of pegmatites. Note the biotite-rich reaction boundary that developed in the metawacke at the contact with the pegmatite that points to a disequilibrium between both lithologies during intrusion of the pegmatites probably during the retrograde *P-T* path; (G) relationships between pegmatites and the S_2 foliation. Note the dike crosscutting S_2 and its apophyses injected in the foliation; (H) "giraffe" pegmatite characterized by an assemblage of rounded quartz porphyroblasts and interstitial feldspar; (I) sigmoidal NW-SE–trending quartz vein emplaced under an extensional regime; (J) thin and straight chlorite-coated fracture crosscutting a pegmatite. Abbreviations: Ab—albite; Apy—arsenopyrite; Bt—biotite; Chl—chlorite; Di—diopside; Fsp—feldspar; Po—pyrrhotite; Py—pyrite; Qtz—quartz; Tur—tourmaline.

domain 1; Fig. 2A). The S_2 foliation is steeply dipping (43–88°), at a low angle to subparallel to bedding, and wraps around the Cheechoo intrusion, where it varies from NE- to W-striking (Fig. 2A). It is marked by biotite and overprinted by syn- to late-S_2 garnet, amphibole, and sillimanite porphyroblasts and contains a down-dip mineral lineation (Figs. S2A and 6). Steeply plunging mesoscopic asymmetric F_2 folds are locally developed and have an axial-planar S_2 foliation. In the intrusion, mafic dikes are also folded (F_2) and affected by the S_2 foliation. Locally, in the Ab-Amp-Di-altered pluton, a distinct banding is imparted by alternating granoblastic and recrystallized quartz-albite and amphibole(-diopside)-rich layers that cut the folded mafic dikes. This banding is NW-SE–trending, steeply dipping (63–88°), and is also present elsewhere in the Cheechoo intrusion in zones of high strain developed along less competent mafic dikes.

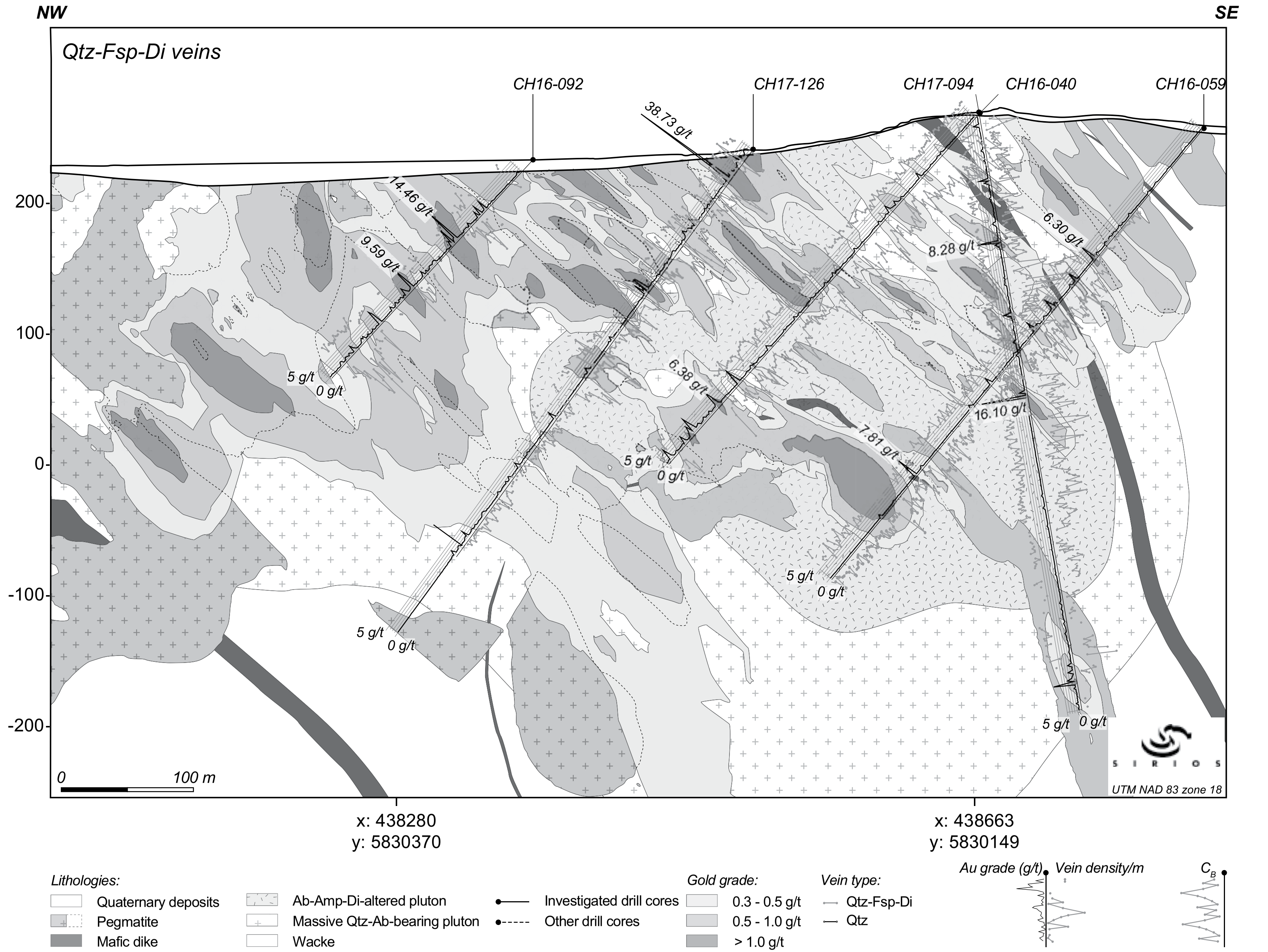

Figure 5. SE-NW cross section across the Cheechoo pluton passes through the drill cores investigated in this study (modeled from drill core data by Sirios Resources, Inc.). The trace of the cross section is represented in Figure 1C. The gold grades are represented on the drill cores along with the vein density and average number of connections per branch (C_B parameter) for Qtz-Fsp-Di veins. Same parameters are reported for Qtz veins on Figure S3 (see footnote 1). Note the decrease of gold grade background values in the albite-amphibole-diopside-altered pluton. Abbreviations: Ab—amphibole; Amp—amphibole; Di—diopside; Fsp—feldspar; Qtz—quartz.

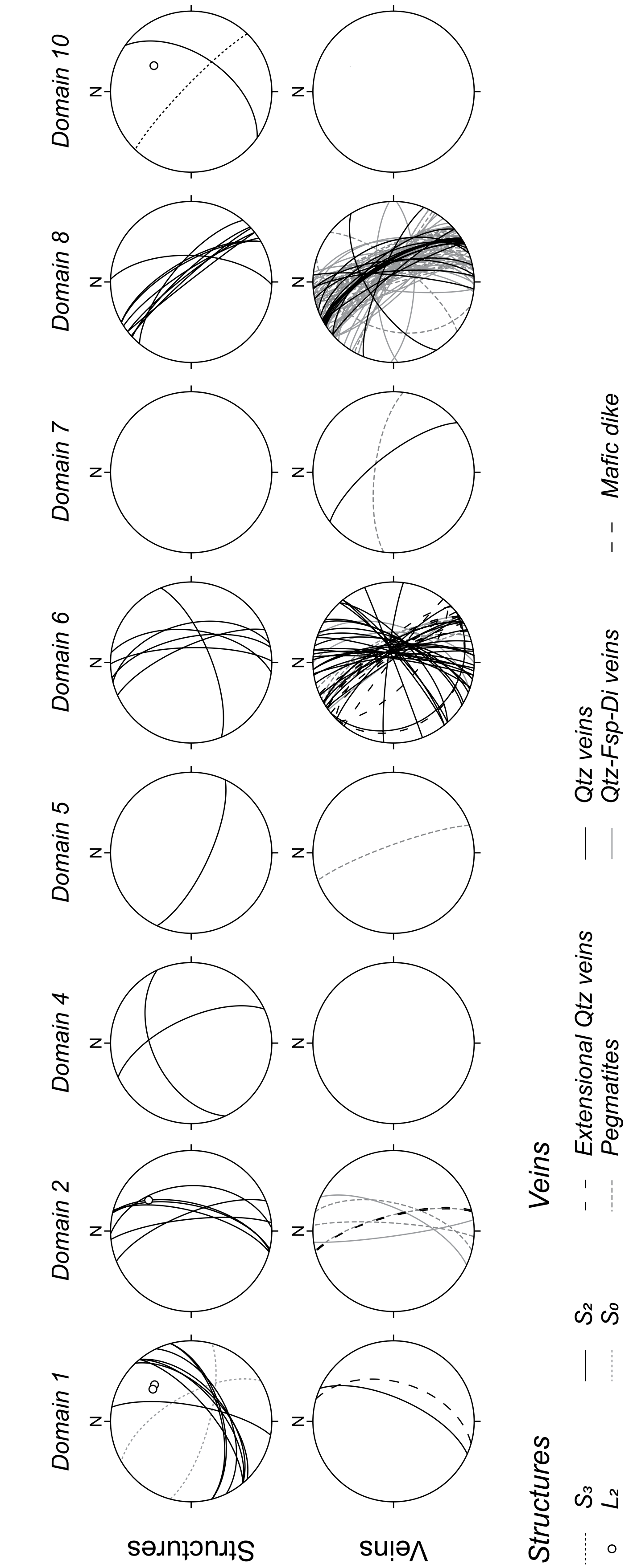

Figure 6. Structural measurements obtained on the main stripped area of the Cheechoo pluton are shown. The numbers of structural zones are reported on Figure 2. Abbreviations: Di—diopside; Fsp—feldspar; Qtz—quartz.

Pegmatites are mostly present in the Ab-Amp-Di-altered facies and in the strongly foliated Bt-bearing facies of the intrusion (Fig. 2A) and show a variety of structures. Elongated straight dikes are steeply-dipping, NW-SE–trending with a significant clockwise reorientation from W to E toward a N-S trend (Figs. 2 and S4). In addition, other (sub-) orthogonal pegmatite dikes are found between and in textural continuity with these elongated dikes (Fig. 2A). The former show ptygmatic and both Z- and S-folds that are indicative of a contraction perpendicular to the dikes (Fig. 2A). The pegmatites are parallel to or cut the S_2 foliation, whereas tourmalinization associated with pegmatite emplacement replaces late- or post-S_2 aluminosilicate porphyroblasts. This suggests that the bulk of D_2-related strain and associated peak metamorphism predates the emplacement of the pegmatites.

In the NE-SW–trending cross section that passes through the main stripped area (Fig. 3), the Cheechoo intrusion shows a megascopic fold with a long wavelength (>500 m) and an axial plane steeply dipping toward the SW. It is associated with folding of mafic dikes and the S_2 foliation and some of the syn-kinematic pegmatites that show a shallow apparent dip in the SW and a steep dip in the NE. In the intrusion, part of the hinge zone of the megascopic fold is occupied by the albite-altered facies of the pluton (Fig. 3). Similar structures are observed on the NW-SE–trending cross section presented in Figure 5. However, the trace of the S_2 foliation is not available on this section and does not allow a structural reconstruction like that proposed for the NE-SW–trending one.

An S_3 crenulation cleavage is locally well developed in the metasedimentary rocks from the main stripped area. It is generally at high-angle to S_2, steeply dipping toward the NE (structural domain 10; Figs. 2A and 6), and associated with open to closed F_3 folds. In the Cheechoo intrusion, the S_3 foliation is marked by biotite and also affects the pegmatite dikes. Along the eastern contact of the granodiorite with the metasedimentary rocks, a 2–5-m-thick, N-striking and E-dipping high strain zone shows well-developed and subparallel S_2 and S_3 foliations as well as asymmetric (Z-shaped) F_3 folds. In this zone, earlier ductile fabrics are cut by a late 10-cm-wide brittle fault and related quartz veins. This brittle fault zone is associated with the formation of chlorite-coated fracture networks and the chloritization of biotite. Within ~20 m to the east of this deformation zone, N-NE–trending pegmatite dikes are buckled into Z-shaped ptygmatic folds, whereas S-SE–trending dikes are boudinaged (Fig. 2A), which is a geometry compatible with a dextral sense of shear during D_3 following dike emplacement along the eastern margin of the intrusion. Elsewhere, within the Cheechoo intrusion, the pegmatites locally accommodate dextral shearing during their emplacement, prior to, or during D_3.

Vein Reorientation

The Qtz-Fsp-Di and Qtz veins are oblique to subparallel to the S_2 foliation (Fig. 6). To a few exceptions, these veins are moderately to steeply dipping (generally 42–90°), but their strike is variable. In the banded altered facies of the intrusion, Qtz-Fsp-Di veins show a mean strike of 297° (between 137° and 359°, $n = 34$) and a mean dip of 73° (between 45° and 89°) (structural domains 7 and 8; Figs. 2A and 6; Table S1). In the same facies, the Qtz veins have a mean strike of 326° (between 238° and 356°, $n = 19$) and a mean dip of 70° (between 49° and 83°) (structural domains 7 and 8; Figs. 2A and 6; Table S1).

In the central part of the outcrop, the granodiorite is massive and shows a quartz-albite alteration. The S_2 foliation is subtle. This facies hosts the highest proportion of Au-bearing veins (Qtz-Fsp-Di and Qtz veins; Fig. 2A), which form dense networks that show a progressive reorientation following a clockwise path from a NW-SE to ESE-WNW orientation (structural domain 6; Figs. 2 and 6). This reorientation is in response to a dextral shearing and is also shown locally at the mesoscopic scale.

SPATIAL AND STATISTIC GOLD GRADE DISTRIBUTION

Main Stripped Area

At the scale of the main stripped area, the gold mineralization is mainly present in both the contact zone between the pluton and the wacke and in the massive Qtz-Ab-altered facies from the central part, where veins cut the intrusion. The latter is the zone with the highest density of Qtz-Fsp-Di and Qtz veins and where these veins underwent a reorientation (Fig. 2).

Cross Sections

At the scale of the investigated drill core cross sections (Fig. 5), the gold grade values in the intrusion were compiled into a gold grade vs. cumulative frequency diagram following the method of Taner and Trudel (1991) (Fig. 7A). The grade distribution shows an inflection around 1 g/t that allows discrimination of two distinct grade populations (Taner and Trudel, 1991). Population A is defined by values below 1 g/t and shows a lognormal distribution (Fig. 7B). On the contrary, population B is defined by values above 1 g/t (and up to 110 g/t) and shows a chaotic distribution that is interpreted to reflect a nugget effect (Fig. 7C). Such distinct distributions have been interpreted to reflect two mineralizing events (Sinclair, 1976; Taner and Trudel, 1991).

The spatial distribution of the gold mineralization in the cross sections is represented as interpolated gold grade envelopes (Figs. 3 and 5). These envelopes follow the general pattern of deformation in the intrusion and present shapes that reflect their folding as for mafic dikes (Figs. 3 and 5). These envelopes are continuous both inside and outside of the Ab-Amp-Di-altered facies of the pluton (Figs. 3 and 5). Outside of this Ab-Amp-Di-altered facies, the gold grade envelopes are widespread and include both sparse high-grade (1 g/t Au) and very high-grade (up to 38.73 g/t Au) mineralization (Figs. 3 and 5). On the contrary, in the Ab-Amp-Di-altered facies and more locally in the pegmatites, the gold grade envelopes are much narrower and characterized by a bimodal distribution of gold grades (Figs. 3 and 5). This is shown by the discrete, very high-grade values with no to slight background; this pattern reflects nugget effects.

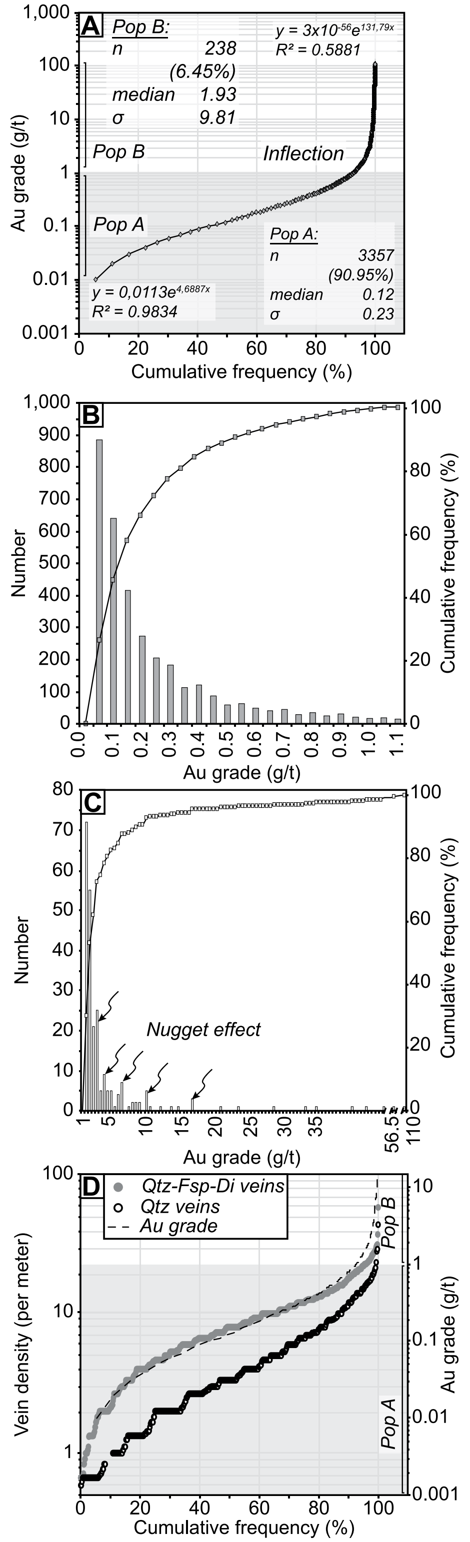

Figure 7. Distribution of gold grade values obtained on drill cores samples of pluton from the Cheechoo deposit (unpublished data are from Sirios Resources, Inc., obtained on drill cores CH14-016, CH15-023, CH15-025, CH15-028, CH16-025E, CH16-031, CH16-040, CH16-059, CH16-092, CH16-093, CH17-094, CH17-126, CH17-135, CH17-137, CH17-141, CH17-143, CH17-144, CH17-145). (A) Gold grade vs. cumulative frequency diagram after Taner and Trudel (1991). The inflection in the distribution around 1 g/t distinguishes two populations of gold grades. (B) Lognormal distribution of the population A of gold grades (<1 g/t). (C) Chaotic distribution of the population B of gold grades (>1 g/t) that witness nugget effects after a gold remobilization (see text for details). (D) Comparison between the density of Qtz-Fsp-Di and Qtz veins and gold grades for the drill core interval studied. Note the matching between the distribution of Qtz-Fsp-Di vein density (and to a minor extent of Qtz veins) and the population A of gold grades (<1 g/t) that points to direct control of this population by the vein networks. Abbreviations: Di—diopside; Fsp—feldspar; Pop A/B—population A/B of gold grades; Qtz—quartz.

DENSITY, TOPOLOGY AND CONNECTIVITY OF VEIN NETWORKS AND THEIR LINK WITH THE GOLD GRADE

Main Stripped Area

On the main stripped area, where the full length of structures is visible, the topology of Qtz-Fsp-Di and of Qtz veins has been investigated on two representative zones for each vein network (Figs. 2A and 8). For the latter, one zone with several visible gold occurrences has been chosen, and the other one is barren to slightly mineralized (Fig. 2A). Plotted in a ternary I-Y-X nodes diagram, the results fall within the fields of those determined by Turlin et al. (2019b) on the same vein networks on drill core samples (Fig. 8). The two investigated Qtz-Fsp-Di vein zones are from two distinct facies: the Qtz-Ab-altered facies and the Ab-Amp-Di-altered facies (Fig. 2A). Both zones yielded similar I-Y-dominated networks with a very low proportion of X nodes (<1.4%; Fig. 8; Table S2) and high connectivity as shown by the average number of connections per branch (C_B parameter; see Appendix A for details) of 1.40 (Table S2). The two Qtz vein zones also yielded I-Y-dominated networks with a very low proportion of X nodes (<6%; Fig. 8; Table S2) but higher connectivity as shown by their C_B parameter, which ranges between 1.58 and 1.68 (Table S2). The Qtz vein zone associated with visible gold is the one that shows the lowest connectivity (zone 1; Figs. 2A and 8) in response to a lower proportion of Y nodes.

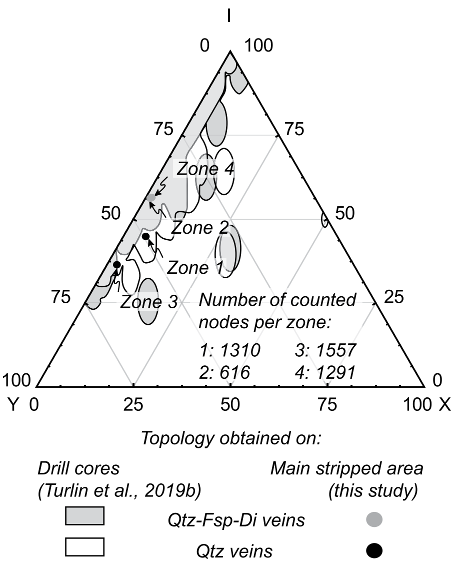

Figure 8. Ternary diagram shows the node type proportion for the Qtz-Fsp-Di veins, Qtz veins, and pegmatites measured on the main stripped area compared to data obtained from the same vein networks measured on drill cores reported by Turlin et al. (2019b). To be noted are the similar results obtained in both cases, which therefore validates the use of the topological approach on both outcrops and drill cores. Abbreviations: Di—diopside; Fsp—feldspar; Qtz—quartz.

Cross Sections

The density of Qtz-Fsp-Di and Qtz veins has been investigated on the drill cores presented in the cross section of Figure 5. In a vein density vs. cumulative frequency diagram, the density of Qtz-Fsp-Di veins shows the same distribution of gold grades (<1 g/t; Fig. 7D) as population A. The density of Qtz-Fsp-Di veins is characterized by a strong increase in low density values (Fig. 7D). The difference between the curves of gold grade distribution and the density of Qtz-Fsp-Di veins appears to be around 1 g/t, i.e., where the gold grade distribution changes from a continuous lognormal one to a discrete distribution dominated by nugget effects. The distribution of the density of Qtz veins is characterized by a more progressive increase than that of Qtz-Fsp-Di veins (Fig. 7D).

Similarly, the topology of Qtz-Fsp-Di and Qtz veins has been measured on the same drill cores. As for the two-dimensional investigations on the main stripped area, results show that both networks are dominated by I-Y nodes with minor proportions of X nodes (Fig. S5; see footnote 1). The increase of Y nodes, i.e., of connectivity, is associated with increasing gold grades (Fig. S5). The topology obtained outside and inside of the Ab-Amp-Di-altered facies is similar (Fig. S5).

When plotted along the investigated drill cores on the cross section in Figure 5, the distribution of the density and C_B parameter (see Appendix A for details) of Qtz-Fsp-Di and Qtz veins does not vary inside or outside of the Ab-Amp-Di-altered facies. Accordingly, it only corresponds to gold grades outside of the Ab-Amp-Di-altered facies (Fig. 5).

DISCUSSION

Distribution of Metal Grades: Evidence for Two Mineralization or Remobilization Events

The investigation of the gold grade distribution in the Cheechoo deposit shows the existence of two distinct populations highlighted by an inflection in the cumulative frequency (Fig. 7A). Two distinct grade populations suggest that two mechanisms of gold precipitation were involved that possibly represent two distinct mineralization or remobilization events (Sinclair, 1976; Taner and Trudel, 1991). Several hypotheses can be proposed for such mechanisms. The first hypothesis is that two gold mineralizing events succeeded one another with no genetic link. The second hypothesis is that an early gold stock was partially remobilized during prograde metamorphism and/or magmatism. This hypothesis seems reasonable as it has been invoked in previous works to explain the genesis of visible gold grains by remobilization in hypogene hydrothermal environments (Hough et al., 2007; Butt et al., 2020; Voisey et al., 2020). Further petrogeochemical investigations of mineralized zones and ore minerals are required to confirm or reject this hypothesis.

Vein Density and Topological Characterization of a Metamorphosed Stockwork

Massive Qtz-Ab-Altered Facies

Visible gold particles are present in both Qtz-Fsp-Di and Qtz veins (Figs. 2A and 4C; Fontaine et al., 2018; Turlin et al., 2019b). These veins are affected by F_2 folds, they are transposed into the S_2 foliation (Fig. 4B), and their selvages contain K-feldspar, amphibole, and diopside porphyroblasts. They show a dextral reorientation in the central part of the main stripped area (Fig. 2). These features demonstrate that these veins predate high-grade metamorphism and are pre- to early-D_2 (Figs. 4A–4B). The cumulative frequency of the Qtz-Fsp-Di vein density and gold grades for population A, i.e., below 1 g/t, are the same (Fig. 7D). These statistical parameters suggest that gold grades of population A are controlled by the Qtz-Fsp-Di veins. The strong increase in the proportion of Qtz-Fsp-Di veins at low densities indicates that these veins formed at an elevated rate of propagation up to a saturation value that is marked by the slower increase of their proportion at high density values (Fig. 7D; e.g., Roberts et al., 1999). On the contrary, the slower increase of the proportion of Qtz veins at low density values (Fig. 7D) is consistent with their emplacement after the Qtz-Fsp-Di veins in a vein-saturated environment in which they nucleated on preexisting structures (e.g., Roberts et al., 1999).

Gold shows a variable distribution that depends on the facies of the intrusion as shown on the cross section presented in Figure 5. The massive Qtz-Ab-altered facies shows widespread low gold values (<0.3 g/t), relatively large zones of higher gold values (>0.3 and <0.5 g/t), and few elevated values (>1.0 g/t) that reach up to 38.73 g/t (Fig. 5). These features suggest that gold grade population A (<1 g/t) is well-developed in the massive Qtz-Ab-altered facies. Moreover, in this facies, elevated values locally occur and are generated by important nugget effects (Fig. 5). These high-grade samples are characterized by narrow grade envelopes with gold values that are higher than in the rest of the massive Qtz-Ab-altered facies (Fig. 5). These elevated values correspond to gold grade population B (>1 g/t). Accordingly, the massive Qtz-Ab-altered facies is characterized by populations of both grades.

In the massive Qtz-Ab-altered facies, zones with the highest gold grades (~1.0–38.73 g/t) also correspond to zones of high density and connectivity (C_B parameter) of Qtz-Fsp-Di (Fig. 5) and Qtz veins (Fig. S3). Hence, in zones of high vein density and connectivity, one would expect that gold grades may reach elevated values typical of population B, i.e., above 1 g/t. Similarly, where the density and connectivity of the vein networks decrease, the gold grades are also expected to decrease down to values typical of population A, i.e., below 1 g/t. The relationships between vein density, topology, and gold grades are also documented at the scale of the main stripped area, where most of the mineralization that is identified on the basis of visible gold and sulfides is concentrated in the central part (structural domain 6, Figs. 2A and 6). This zone corresponds to the highest density of Qtz-Fsp-Di veins (Figs. 2A and 9). On this outcrop, the topology investigations carried out on these vein networks over areas of a few square meters yielded similar results as those obtained from drill cores (Figs. 8 and S5). These results demonstrate that the density and connectivity of Qtz-Fsp-Di veins control the first mineralizing event. Where these networks show relatively low density and connectivity, gold values are relatively low, i.e., characteristic of population A. On the contrary, a high density and connectivity of Qtz-Fsp-Di veins leads to the elevated gold grades characteristic of population B.

Amp-Ab-Di-Altered Facies

The Amp-Ab-Di-altered facies is characterized by gold grades with an erratic gold distribution and limited background values below 0.3 g/t as shown by the thin grade envelopes centered on a few elevated values that reach up to 110 g/t (Fig. 5). Such features indicate that the distribution of gold grades in this facies is essentially dominated by population B (>1 g/t).

The gold mineralizing event that is expressed in the Amp-Ab-Di-altered facies can have two distinct origins, namely, a new gold input or remobilization of a previous gold stock. The Amp-Ab-Di-altered facies is more altered than the massive Qtz-Ab-altered one. Accordingly, the stronger proportion of pre-metamorphic hydrated minerals from the Amp-Ab-Di-altered facies could have released more fluids than the massive Qtz-Ab-altered one during regional peak metamorphism at amphibolite facies. This fluid release would have enhanced the remobilization of gold that would have been reconcentrated as visible gold grains (e.g., Tomkins, 2007). This hypothesis is consistent with the preservation of the density and connectivity of the gold-bearing Qtz-Fsp-Di veins in both the massive Qtz-Ab- and Amp-Ab-Di-altered facies during regional metamorphism and deformation. Accordingly, we propose that the distribution of gold grades in the Amp-Ab-Di-altered facies is due, in part, to gold remobilization.

Pegmatites

Pegmatites present a similar distribution of gold grades as the Amp-Ab-Di-altered facies, i.e., dominated by randomly distributed and erratic gold values that can reach several g/t. Pegmatites crosscut previous vein networks, i.e., Qtz-Fsp-Di and Qtz veins. They present elongation features that can represent primary injection structures such as bead strings, as was proposed for the Cap de Creus (NE Spain) by Bons et al. (2004). These authors show that apparent boudinage can be caused by injection and subsequent local expansion and collapse at the edges of the magmatic body. This type of mechanism can only appear when the magma is emplaced under ductile conditions and low cooling rates (Bons et al., 2004). These conditions allow the formation of bead strings by ductile flow of the host rock (Bons et al., 2004). However, even though the thermal conditions are met in the study area, S_2-parallel pegmatites from the Cheechoo intrusion that show elongation features are also in textural continuity with folded pegmatites that are oblique relative to S_2 (Figs. 2 and 4F). In addition, both S_2-parallel and folded pegmatites lack evidence for solid-state or intracrystalline deformation, and the latest pegmatitic dikes are parallel to the S_3 foliation (Figs. 2A and 9). These structural features are typical of lower crustal ductile environments (e.g., Brisbin, 1986). They define an anisotropic regime of deformation with an apparent subhorizontal extension and minimum principal stress (σ_3) direction. The associated calculated elongation direction shows a clockwise rotation with azimuths that range from WNW-ESE in the southern part of the Ab-Amp-Di-altered facies to NNW-SSE in the northern part of the strongly foliated Bt-bearing facies (Fig. 2B). The folded pegmatites are at low angle relative to the calculated maximum principal stress (σ_1) direction (Figs. 2 and 4F). Accordingly, the shortening features observed for pegmatites from the Cheechoo deposit, as well as the lack of solid-state fabric, are interpreted as representing their syn-kinematic injection under ductile conditions following peak metamorphism (see discussions in Turlin et al., 2017, 2018, 2019a).

Genetic Model

We propose in Figure 9 a structural evolution model of the genesis of the prograde stockwork that includes the timing of gold input and remobilization(s). The Qtz veins crosscut the Qtz-Fsp-Di veins, both show structural features that allow them to be attributed to a pre- to early-D_2 stage (Fig. 9), and they share a similar albitic alteration halo. This is consistent with the type of complex and protracted hydrothermal activity that would generate both vein types and hydrothermal alteration assemblages. Moreover, the Qtz-Fsp-Di and Qtz vein networks show a conservation of density, topology, and connectivity between the massive Qtz-Ab-altered facies and the Ab-Amp-Di-altered facies as demonstrated both on the main stripped area (Figs. 2A and S5) and in the cross section of Figure 5. The similar results obtained on two-dimensional (horizontal) and on one-dimensional (vertical) drill core investigations indicate that the connectivity has an isotropic character. The saccharoidal texture and presence of diopside and amphibole porphyroblasts in the hydrothermally altered intrusion and metasedimentary rocks and in Qtz-Fsp-Di veins reflect a secondary metamorphic mineral assemblage that may be associated with the recrystallization of an earlier hydrothermal system at amphibolite facies conditions. This is consistent with the amphibolite *P-T* conditions reached in the area (Fontaine et al., 2018; Fontaine, 2019). Such features are typical of gold deposits in amphibolite facies metamorphic belts (McCuaig and Kerrich, 1998; Eilu et al., 1999; Tomkins, 2007). Accordingly, even though further petrogenetic documentation is needed to confirm this hypothesis, we favor a model in which early pervasive hydrothermal alteration and associated veins (Qtz-Fsp-Di and Qtz veins) were metamorphosed to form the sodic and calc-silicate facies in the intrusion (Fig. 9).

The first gold input would have been associated with the early pervasive hydrothermal alteration (Fig. 9) as shown by the control of the gold grades in the massive Qtz-Ab-altered facies by the density and connectivity of the Qtz-Fsp-Di veins. In the massive Qtz-Ab-altered facies, the lowest density and connectivity of these veins is associated with the lowest gold values. Accordingly, both populations A and B are associated with this gold input. The subsequent regional metamorphism would have promoted fluid release and mobilization of the previous gold stock especially from the Amp-Ab-Di-altered facies.

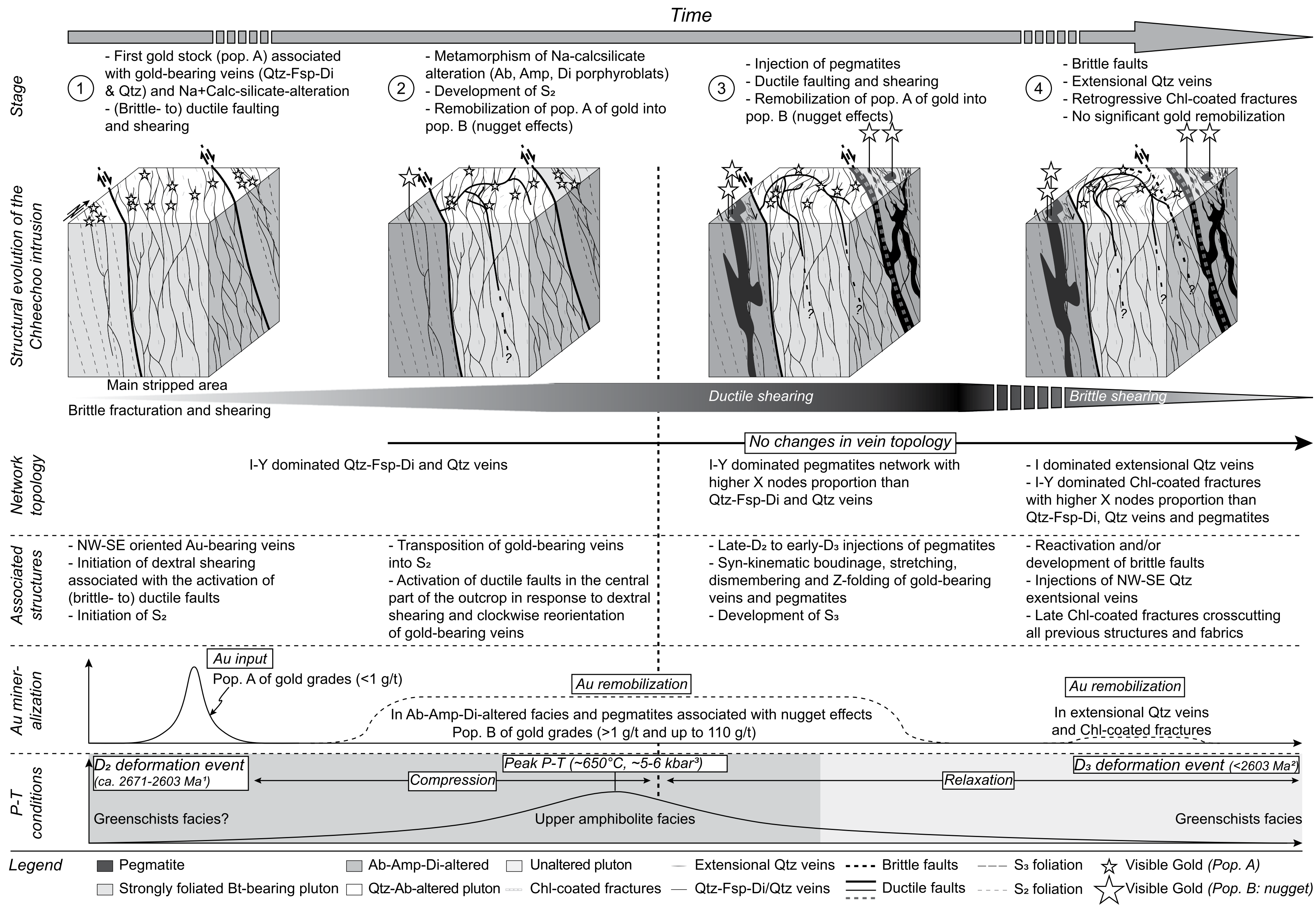

Figure 9. Schematic model shows the structural evolution of the main stripped area of the Cheechoo pluton associated with several successive vein injections and structures evolving with *P-T* conditions and distinct gold mineralization events. Abbreviations: [1]—(Dubé et al., 2011; Ravenelle, 2013; Fontaine et al., 2018); [2]—(Ravenelle et al., 2010); [3]—(Bandyayera et al., 2010; Ravenelle et al., 2010; Fontaine, 2019); Chl—chlorite; Di—diopside; Fsp—feldspar; Pop.—population of gold grade; Qtz—quartz.

It is proposed that, in this facies, gold was in part remobilized to form population B (Fig. 9). Gold remobilization was also associated with syn-kinematic late-D_2 to early-D_3 pegmatites, which are interpreted to have scavenged part of the initial gold stock during magma ascent and emplacement (Fig. 9).

The results presented in this study show that the grade vs. cumulative frequency diagram of Taner and Trudel (1991) (Fig. 7) cannot be seen as a means for discriminating grade values associated with specific mineralizing events. Indeed, we show that in the Cheechoo deposit, the population B of gold grades, which is identified on the basis of inflection points in this diagram (Fig. 7), does not represent in itself a new gold mineralizing event. On the contrary, this population B is composed of values that belong to both the first mineralizing event and to its remobilization. Accordingly, the use of the grade vs. cumulative frequency diagram of Taner and Trudel (1991) must be used as a tool for identifying gold grade populations that can afterward be interpreted in terms of processes.

CONCLUSIONS

In this study, we show that the coupling of field geology, gold grade distribution, vein density, topology, and connectivity allows for a better understanding of the metallogenic history of a deposit even if it has undergone high-grade metamorphism and deformation. Our results obtained on the Cheechoo stockwork show that two steps may be distinguished in the evolution of a metamorphosed stockwork as indicated by the bimodal gold grade distribution. This distribution, coupled with field relationships, vein mineralogy, and vein density and connectivity, shows that the Qtz-Fsp-Di veins control the input of a first gold stock in the Cheechoo deposit. This first stock was associated with hydrothermal alteration that was metamorphosed to sodic and calcsilicate facies during peak metamorphism. It was further locally concentrated in a smaller volume of the pluton in response to vein reorientation associated with dextral shearing during regional deformation and metamorphism. The geometry of the stockwork was preserved during this shearing and vein reorientation. Moreover, the multi-method approach yields evidence for isotropic behavior of the topology, and therefore of the connectivity, of the stockworks during regional deformation.

The same methodology also suggests evidence for a gold remobilization event. The gold distribution associated with this event is characterized by a strong nugget effect, which is found both in the Ab-Amp-Di-altered facies and locally in the pegmatites. The development of porphyroblasts of albite, actinolite, diopside, and titanite in these hydrothermally altered facies suggests metamorphism up to amphibolite facies. This event is interpreted to have been associated with fluid release during metamorphism, which thus promoted the remobilization of the first gold stock. Similarly, gold-bearing pegmatites showing random and locally high-grade gold mineralization would have scavenged part of the first gold stock during magma ascent and emplacement in the Cheechoo pluton.

Accordingly, we provide evidence that the development of a stockwork is not restricted to the retrograde evolution of magmatic-hydrothermal or metamorphic systems, but that it can happen during the early stages of regional prograde metamorphism. Moreover, the results provide new clues for the characterization of successive veining or fracturing events and for predicting the loci of mineralization in such systems. The latter is of prime importance in terms of the exploration, evaluation, and exploitation of a deposit. Accordingly, this study opens new avenues regarding the characterization of hydrothermal deposits and of vein networks even if they have undergone high-grade metamorphism.

APPENDIX A. CALCULATIONS OF NETWORK TOPOLOGY

Considered in a two-dimensional plane, a vein is represented by a finite line or trace. It is composed of one or more branches that ends by a node at each termination (Fig. A1; Sanderson and Nixon, 2015). Three categories of nodes are defined, namely isolated tips (I), abutments or splays (Y), or intersections (X) (Fig. A1; Manzocchi, 2002; Mäkel, 2007; Sanderson and Nixon, 2015). The network topology is defined on the basis of the relative proportions of these nodes.

A vein is divided into branches that are characterized by two nodes. I nodes contribute to one branch, Y nodes to three branches, and X nodes to four branches. Therefore, the number of branch (N_B) is (the following equations are from Sanderson and Nixon, 2015):

$$N_B = 1/2(N_I + 3N_Y + 4N_X) \quad (1)$$

where N_I, N_Y, and N_X are the number of counted I, Y, and X nodes, respectively.

The average number of connections per branch (C_B) is given by:

$$C_B = (3N_Y + 4N_X)/N_B \quad (2)$$

This parameter is a proxy of the connectivity of a vein network (Sanderson and Nixon, 2015). It varies between 0 (unconnected network) and

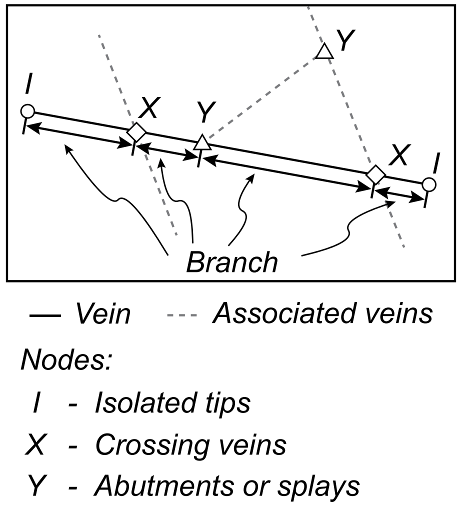

Figure A1. Schematic representation shows the topologic approach that illustrates the relationships between veins from a similar population and the various types of counted nodes used to evaluate network topologies and connectivity (adapted from Sanderson and Nixon, 2015; Turlin et al., 2019b).

2 (fully connected network) (Sanderson and Nixon, 2015). A percolation threshold is set by Sanderson and Nixon (2018) at a C_B value of ~1.56. However, Turlin et al. (2019b) argued that some form of connectivity can be reached below this percolation threshold.

ACKNOWLEDGMENTS

The authors thank Sirios Resources, Inc., and Dominique Doucet, who allowed access to drill core samples and supported this study. The authors are grateful to Jiří Žák and Ross N. Mitchell for constructive comments that significantly improved the manuscript and to Rob Strachan for editorial handling. This study was funded by Collaborative Research and Development (CRD) grant 538419-2018 supported by the Natural Sciences and Engineering Research Council of Canada (NSERC) in partnership with Sirios Resources, Inc.

REFERENCES CITED

André-Mayer, A.-S., and Sausse, J., 2007, Thickness and spatial distribution of veins in a porphyry copper deposit, Rosia Poieni, Romania: Journal of Structural Geology, v. 29, no. 10, p. 1695–1708, https://doi.org/10.1016/j.jsg.2007.06.010.

Bandyayera, D., and Fliszár, A., 2007, Géologie de la région de la baie Kasipasikatch (33C09) et du lac Janin (33C16): Ministère des Ressources naturelles et de la Faune (MRNF), RP 2007–05, 15 p.

Bandyayera, D., and Lacoste P., 2009, Géologie de la région du lac de Rotis (33C10), du lac Bernou (33C11) et du lac Boyd (33C15): Ministère de l'Énergie et des Ressources naturelles, RP-2009-06, 15 p.

Bandyayera, D., Rhéaume, P., Maurice, C., Bédard, É., Morfin, S., and Sawyer, E., 2010, Synthèse géologique du secteur du réservoir Opinaca, Baie-James: Ministry of Ministère des Ressources naturelles et de la Faune (MRNF), RG 2010–02, 46 p.

Blenkinsop, T.G., Oliver, N.H.S., Dirks, P.G.H.M., Nugus, M., Tripp, G., and Sanislav, I., 2020, Structural geology applied to the evaluation of hydrothermal gold deposits: Reviews in Economic Geology, v. 21, p. 1–23, https://doi.org/10.5382/rev.21.01.

Bons, P.D., Druguet, E., Hamann, I., Carreras, J., and Passchier, C.W., 2004, Apparent boudinage in dykes: Journal of Structural Geology, v. 26, no. 4, p. 625–636, https://doi.org/10.1016/j.jsg.2003.11.009.

Brisbin, W.C., 1986, Mechanisms of pegmatite intrusion: The American Mineralogist, v. 71, p. 644–651.

Buchan, K.L., Mortensen, J.K., and Card, K.D., 1993, Northeast-trending Early Proterozoic dykes of southern Superior Province: Multiple episodes of emplacement recognized from integrated paleomagnetism and UPb geochronology: Canadian Journal of Earth Sciences, v. 30, no. 6, p. 1286–1296, https://doi.org/10.1139/e93-110.

Butt, C.R.M., Hough, R.M., and Verrall, M., 2020, Gold nuggets: The inside story: Ore and Energy Resource Geology, v. 4–5, no. 100009, https://doi.org/10.1016/j.oreoa.2020.100009.

Cadéron, S., 2003, Interprétation tectonométamorphique du Nord de la Province Supérieur, Québec, Canada [thèse de doctorat]: Montréal, Canada, Université du Québec à Montréal, 343 p.

Cleven, N.R., Guilmette, C., Davis, D.W., and Côté-Roberge, M., 2020, Geodynamic significance of Neoarchean metasedimentary belts in the Superior Province: Detrital zircon U-Pb LA-ICP-MS geochronology of the Opinaca and La Grande subprovinces: Precambrian Research, v. 347, no. 105819, https://doi.org/10.1016/j.precamres.2020.105819.

Corriveau, L., Mumin, A.H., and Setterfield, T., 2010, IOCG environments in Canada: Characteristics, geological vectors to ore and challenges, *in* Porter, T.M., ed., Hydrothermal Iron Oxide Copper-Gold & Related Deposits: Adelaide, Australia, A Global Perspective 4, Advances in the Understanding of IOCG Deposits, PGC Publishing, p. 311–344.

Côté-Roberge, M., 2018, Contexte tectonométamorphique du nord-ouest du Complexe de Laguiche, sous-province d'Opinaca, Eeyou Itschee Baie-James, [MSc thesis]: Quebec City, Canada, Université Laval, 216 p.

David, J., Vaillancourt, D., Bandyayera, D., Simard, M., Dion, C., Goutier, J., and Barbe, P., 2010, Datations U-Pb effectuées dans les sousprovinces d'Ashuanipi, de La Grande, d'Opinaca et d'Abitibi en 2008–2009: Quebec, Canada, Ministère de l'Énergie et des Ressources naturelles, RP 2010-11(A), 37 p.

de Joussineau, D., and Aydin, A., 2007, The evolution of the damage zone with fault growth in sandstone and its multiscale characteristics: Journal of Geophysical Research: Solid Earth, v. 112, no. B12401, https://doi.org/10.1029/2006JB004711.

Dubé, B., Ravenelle, J.-F., McNicoll, V., Malo, M., Creaser, R., Nadeau, L., and Simoneau, J., 2011, The world-class Roberto gold deposit, Éléonore property, James Bay area, Québec: Insights from geology and geochronology, *in* Proceedings, Joint Annual Meeting of the Geological Association of Canada-Mineralogical Association of Canada-Society of Economic Geologists-Society for Geology Applied to Mineral Deposits: Ottawa, Canada.

Eilu, P., Mathison, C.I., Groves, D.I., and Allardyce, W.J., 1999, Atlas of alteration assemblages and zoning in orogenic lode-gold deposits in a variety of host rock and metamorphic settings: Perth, Australia, The University of Western Australia Publication No. 30, 64 p.

Fahrig, W.F., Christie, K.W., Chown, E.H., Janes, D., and Machado, N., 1986, The tectonic significance of some basic dyke swarms in the Canadian Superior Province with special reference to the geochemistry and paleomagnetism of the Mistassini swarm, Quebec, Canada: Canadian Journal of Earth Sciences, v. 23, no. 2, p. 238–253, https://doi.org/10.1139/e86-026.

Fontaine, A., 2019, Géologie des minéralisations aurifères de la mine Éléonore, Eeyou Istchee Baie-James, Province du Supérieur, Québec, Canada [thèse de doctorat]: Québec, Canada, Université du Québec, Institut National de la Recherche Scientifique, Centre Eau Terre Environnement, 468 p.

Fontaine, A., Dubé, B., Malo, M., McNicoll, V., Brisson, T., Doucet, D., and Goutier, J., 2015, Geology of the metamorphosed Roberto gold deposit (Éléonore mine), Baie-James region, Québec: Diversity of mineralization styles in a polyphase tectono-metamorphic setting, *in* Targeting Geoscience Initiative 4: Geological Survey of Canada Open File Report 7852, p. 209–225.

Fontaine, A., Dubé, B., Malo, M., McNicoll, V., Jackson, S.E., Beausoleil, C., Layne, G.D., and Goutier, J., 2017, Geology and insights on the genesis of the world-class Éléonore gold mine, Eeyou Istchee Baie-James, Superior Province, Quebec, Canada, *in* Proceedings of the 14th Biennial Society for Geology Applied to Mineral Deposits Meeting: Québec, Canada, p. 31–34.

Fontaine, A., Dubé, B., Malo, M., Turcotte, J., and Doucet, D., 2018, Geology of the Cheechoo gold property, Eeyou Istchee Baie-James, Superior Province, northern Quebec: Geological Survey Of Canada Open File Report 8403, 25 p., https://doi.org/10.4095/308244.

Franklin, J.M., Sangster, D.M., Lydon, J.W., and Skinner Brian, J.E.D., 1981, Volcanic-associated massive sulfide deposits: Economic Geology, v. 75, p. 485–627.

Fraser, R.J., 1993, The Lac Troilus Gold-Copper deposit, northwestern Quebec: A possible Archean Porphyry system: Economic Geology, v. 88, p. 1685–1699, https://doi.org/10.2113/gsecongeo.88.6.1685.

Gillespie, P.A., Howard, C.B., Walsh, J.J., and Watterson, J., 1993, Measurement and characterisation of spatial distributions of fractures: Tectonophysics, v. 226, p. 113–141, https://doi.org/10.1016/0040-1951(93)90114-Y.

Gillespie, P.A., Johnston, J.D., Loriga, M.A., McCaffrey, K.J.W., Walsh, J.J., and Watterson, J., 1999, Influence of layering on vein systematics in line samples, *in* McCaffrey, K.J.W., Lonergan, L., and Wilkinson, J.J., eds., Fractures, Fluid Flow and Mineralization: Geological Society, London, Special Publication 155, p. 35–56, https://doi.org/10.1144/GSL.SP.1999.155.01.05.

Goodman, S., Williams-Jones, A.E., and Carles, P., 2005, Structural controls on the Archean Troilus Gold-Copper deposit, Quebec, Canada: Economic Geology, v. 100, p. 577–582, https://doi.org/10.2113/gsecongeo.100.3.577.

Goutier, J., Dion, C., Ouellet, M., David, J., and Parent, M., 2000, Géologie de la région des lacs Guillaumat et Sakami (SNRC 33F/02 et 33F/07): Québec, Canada, Ministère des Ressources naturelles et de la Faune (MRNF), Report RG 99-15, 37 p.

Heaman, L.M., 1997, Global mafic magmatism at 2.45 Ga: Remnants of an ancient large igneous province?: Geology, v. 25, no. 4, p. 299–302, https://doi.org/10.1130/0091-7613(1997)025<0299:GMMAGR>2.3.CO;2.

Hooker, J.N., and Katz, R.F., 2015, Vein spacing in extending, layered rock: The effect of synkinematic cementation: American Journal of Science, v. 315, p. 557–588, https://doi.org/10.2475/06.2015.03.

Hooker, J.N., Gomez, L.A., Laubach, S.E., Gale, J.F.W., and Marrett, R., 2012, Effects of diagenesis (cement precipitation) during fracture opening on fracture aperture size scaling in carbonate rocks, *in* Garland, J., Neilson, J.E., Laubach, S.E., and Whidden, K.J., eds., Advances in Carbonate Exploration and Reservoir Analysis: Geological Society, London, Special Publication 370, p. 187–206, https://doi.org/10.1144/SP370.9 .

Hooker, J.N., Laubach, S.E., and Marrett, R., 2013, Fracture-aperture sized frequency, spatial distribution, and growth processes in strata-bounded and non-strata-bounded fractures, Cambrian Mesón Group, NW Argentina: Journal of Structural Geology, v. 54, p. 54–71, https://doi.org/10.1016/j.jsg.2013.06.011.

Hooker, J.N., Laubach, S.E., and Marrett, R., 2018, Microfracture spacing distributions and the evolution of fracture patterns in sandstones: Journal of Structural Geology, v. 108, p. 66–79, https://doi.org/10.1016/j.jsg.2017.04.001.

Hough, R.M., Butt, C.R.M., Reddy, S.M., and Verrall, M., 2007, Gold nuggets: Supergene or hypogene?: Australian Journal of Earth Sciences, v. 54, no. 7, p. 959–964, https://doi.org/10.1080/08120090701488289.

Jébrak, M., 1992, Les gisements d'or des tonalities archéennes (Abitibi, Québec): Mineralium Deposita, v. 27, p. 1–9, https://doi.org/10.1007/BF00196075.

Katz, L.R., Kontak, D.J., Dubé, B., and McNicoll, V., 2017, The geology, petrology, and geochronology of the Archean Côté Gold large-tonnage, low-grade intrusion-related Au(–Cu) deposit, Swayze greenstone belt, Ontario, Canada: Canadian Journal of Earth Sciences, v. 54, p. 173–202, https://doi.org/10.1139/cjes-2016-0007.

Laubach, S.E., Lamarche, J., Gauthier, B.D.M., Dunne, W.M., and Sanderson, D.J., 2018, Spatial arrangement of faults and opening-mode fractures: Journal of Structural Geology, v. 108, p. 2–15, https://doi.org/10.1016/j.jsg.2017.08.008.

Lavenu, A.P.C., and Lamarche, J., 2018, What controls diffuse fractures in platform carbonates? Insights from Provence (France) and Apulia (Italy): Journal of Structural Geology, v. 108, p. 94–107, https://doi.org/10.1016/j.jsg.2017.05.011.

Mäkel, G.H., 2007, The modelling of fractured reservoirs: Constraints and potential for fracture network geometry and hydraulics analysis, *in* Mäkel, G.H., The Modelling of Fractured Reservoirs: Constraints and Potential for Fracture Network Geometry and Hydraulics Analysis: Geological Society, London, Special Publication 292, p. 375–403, https://doi.org/10.1144/SP292.21.

Manzocchi, T., 2002, The connectivity of two dimensional networks of spatially correlated fractures: Water Resources Research, v. 38, no. 9, p. 1-1–1-20, https://doi.org/10.1029/2000WR000180.

Marrett, R., Gale, J.F.W., Gómez, L.A., and Laubach, S.E., 2018, Correlation analysis of fracture arrangement in space: Journal of Structural Geology, v. 108, p. 16–33, https://doi.org/10.1016/j.jsg.2017.06.012.

McCaffrey, K.J.W., and Johnston, J.D., 1996, Fractal analysis of a mineralised vein deposit: Curraghinalt gold deposit, County Tyrone: Mineralium Deposita, v. 31, p. 52–58, https://doi.org/10.1007/BF00225395.

McCuaig, T.C., and Kerrich, R., 1998, P-T-t-deformation-fluid characteristics of lode gold deposits: Evidence from alteration systematics: Ore Geology Reviews, v. 12, no. 6, p. 381–453, https://doi.org/10.1016/S0169-1368(98)00010-9.

McGinnis, R.N., Ferrill, D.A., Morris, A.P., Smart, K.J., and Lehrmann, D., 2017, Mechanical stratigraphic controls on natural fracture spacing and penetration: Journal of Structural Geology, v. 95, p. 160–170, https://doi.org/10.1016/j.jsg.2017.01.001.

Monecke, T., Gemmell, J.B., and Monecke, J., 2001, Fractal distributions of veins in drill core from the Hellyer VHMS deposit, Australia: Constraints on the origin and evolution of the mineralising system: Mineralium Deposita, v. 36, p. 406–415, https://doi.org/10.1007/s001260100161.

Morfin, S., Sawyer, E.W., and Bandyayera, D., 2013, Large volumes of anatectic melt retained in granulite facies migmatites: An injection complex in northern Quebec: Lithos, v. 168, p. 200–218, https://doi.org/10.1016/j.lithos.2013.02.007.

Morfin, S., Sawyer, E.W., and Bandyayera, D., 2014, The geochemical signature of a felsic injection complex in the continental crust: Opinaca Subprovince, Quebec: Lithos, v. 196, p. 339–355, https://doi.org/10.1016/j.lithos.2014.03.004.

Moukhsil, A., 2000, Géologie de la région des lacs Pivert (33C/01), Anatacau (33C/02), Kauputauchechun (33C/07) et Wapamisk (33C/08): Québec, Canada, Ministère des Ressources naturelles, RG 2000-04, 47 p.

Moukhsil, A., Legault, M., Boily, M., Doyon, J., Sawyer, E., and Davis, D.W., 2003, Synthèse géologique et métallogénique de la ceinture de roches vertes de la Moyenne et de la Basse-Eastmain (Baie-James): Québec, Canada, Ministère des Ressources naturelles, de la Faune et des Parcs, ET 2002-06, 55 p.

Narr, W., and Suppe, J., 1991, Joint spacing in sedimentary rocks: Journal of Structural Geology, v. 13, no. 9, p. 1037–1048, https://doi.org/10.1016/0191-8141(91)90055-N.

Ravenelle, J.-F., 2013, Amphibolite facies gold mineralization: An example from the Roberto deposit, Eleonore property, James Bay, Quebec [Ph.D. thesis]: Québec City, Canada, Université du Québec, Institut national de la recherche scientifique, 325 p.

Ravenelle, J.-F., Dubé, B., Malo, M., McNicoll, V., Nadeau, L., and Simoneau, J., 2010, Insights on the geology of the world-class Roberto gold deposit, Éléonore property, James Bay area, Quebec: Geological Survey of

Canada, Current Research 2010-1, 26 p., https://doi.org/10.4095/261482.
Remick, J., 1977, Wemindji area (Municipiality of James Bay), Preliminary report: Ministère des Richesses naturelles, DPV-446, 51 p.
Roberts, S., Sanderson, D.J., and Gumiel, P., 1998, Fractal analysis of Sn-W mineralization from Central Iberia: Insights into the role of fracture connectivity in the formation of an ore deposit: Economic Geology, v. 93, p. 360–365, https://doi.org/10.2113/gsecongeo.93.3.360.
Roberts, S., Sanderson, D.J., and Gumiel, P., 1999, Fractal analysis and percolation properties of veins, *in* McCaffrey, K.J.W., Lonergan, L., and Wilkinson, J.J., eds., Fractures, Fluid Flow and Mineralization: Geological Society, London, Special Publication 155, p. 7–16, https://doi.org/10.1144/GSL.SP.1999.155.01.03
Sanderson, D.J., and Nixon, C.W., 2015, The use of topology in fracture network characterization: Journal of Structural Geology, v. 72, p. 55–66, https://doi.org/10.1016/j.jsg.2015.01.005.
Sanderson, D.J., and Nixon, C.W., 2018, Topology, connectivity and percolation in fracture networks: Journal of Structural Geology, v. 115, p. 167–177, https://doi.org/10.1016/j.jsg.2018.07.011.
Sanderson, D.J., Roberts, S., and Gumiel, P., 1994, A fractal relationship between vein thickness and gold grade in drill core from La Codosera, Spain: Economic Geology, v. 89, p. 168–173, https://doi.org/10.2113/gsecongeo.89.1.168.
Sanderson, D.J., Roberts, S., Gumiel, P., and Greenfield, C., 2008, Quantitative analysis of tin and tungsten bearing sheeted vein systems: Economic Geology, v. 103, p. 1043–1056, https://doi.org/10.2113/gsecongeo.103.5.1043.
Sillitoe, R., 2010, Porphyry copper systems: Economic Geology, v. 105, p. 3–41, https://doi.org/10.2113/gsecongeo.105.1.3.
Simard, M., and Gosselin, C., 1999, Géologie de la région du lac Lichteneger (SNRC 33B): Ministère des Ressources naturelles, RG 98–15, 25 p.
Sinclair, A.J., 1976, Probability graphs in mineral exploration: Nepean, Canada, Association of Exploration Geochemists, Special Volume 4, 95 p.
Solomon, M., 1976, "Volcanic" massive sulphide deposits and their host rocks—a review and an explanation, *in* Wolf, K.H., ed., Handbook of Stratabound and Stratiform Ore Deposits 6: Amsterdam, Elsevier, 21–54, https://doi.org/10.1016/B978-0-444-41406-9.50006-3.
Taner, M.F., and Trudel, P., 1991, Gold distribution in the Val-d'Or Formation and a model for the formation of the Lamaque–Sigma mines, Val-d'Or, Quebec: Canadian Journal of Earth Sciences, v. 28, p. 706–720, https://doi.org/10.1139/e91-061.
Terzaghi, R.D., 1965, Sources of error in joint surveys: Geotechnique, v. 15, no. 3, p. 287–304, https://doi.org/10.1680/geot.1965.15.3.287.
Tomkins, A.G., 2007, Three mechanisms of ore re-mobilisation during amphibolite facies metamorphism at the Montauban Zn-Pb-Au-Ag deposit: Mineralium Deposita, v. 42, p. 627–637, https://doi.org/10.1007/s00126-007-0131-9.
Turlin, F., André-Mayer, A.-S., Moukhsil, A., Vanderhaeghe, O., Gervais, F., Solgadi, F., Groulier, P.-A., and Poujol, M., 2017, Unusual LREE-rich, peraluminous, monazite- or allanite-bearing pegmatitic granite in the central Grenville Province, Québec: Ore Geology Reviews, v. 89, p. 627–667, https://doi.org/10.1016/j.oregeorev.2017.04.019.
Turlin, F., Deruy, C., Eglinger, A., Vanderhaeghe, O., André-Mayer, A.-S., Poujol, M., Moukhsil, A., and Solgadi, F., 2018, A 70 Ma record of suprasolidus conditions in the large, hot, long-duration Grenville Orogen: Terra Nova, v. 30, p. 233–243, https://doi.org/10.1111/ter.12330.
Turlin, F., Vanderhaeghe, O., Gervais, F., André-Mayer, A.-S., Moukhsil, A., Zeh, A., Solgadi, F., and I.P.T.N., 2019a, Petrogenesis of LREE-rich pegmatitic granite dykes in the central Grenville Province by partial melting of Paleoproterozoic-Archean metasedimentary rocks: Evidence from zircon U-Pb-Hf-O isotope and trace element analyses: Precambrian Research, v. 327, p. 327–360, https://doi.org/10.1016/j.precamres.2019.02.009.
Turlin, F., Jébrak, M., De Souza, S., and Turcotte, J., 2019b, Topological characterization of a polyphased gold-bearing vein network: Journal of Structural Geology, v. 128, no. 103872, https://doi.org/10.1016/j.jsg.2019.103872.
Ulrich, T., and Heinrich, C.A., 2002, Geology and alteration geochemistry of the porphyry Cu-Au deposit at Bajo de la Alumbrera, Argentina: Economic Geology, v. 97, no. 8, p. 1865–1888, https://doi.org/10.2113/gsecongeo.97.8.1865.
Voisey, C.R., Willis, D., Tomkins, A.G., Wilson, C.J.L., Micklethwaite, S., Salvemini, F., Bougoure, J., and Rickard, W.D.A., 2020, Aseismic refinement of orogenic gold systems: Economic Geology, v. 115, no. 1, p. 33–50, https://doi.org/10.5382/econgeo.4692.
Watkins, H., Healy, D., Bond, C.E., and Butler, R.W.H., 2018, Implications of heterogeneous fracture distribution on reservoir quality; an analogue from the Torridon Group sandstone, Moine Thrust Belt, NW Scotland: Journal of Structural Geology, v. 108, p. 180–197, https://doi.org/10.1016/j.jsg.2017.06.002.

Science Editor: Rob Strachan
Associate Editor: Yin Changqing

Manuscript Received 27 January 2021
Revised Manuscript Received 7 May 2021
Manuscript Accepted 26 May 2021

Printed in the USA